(2)

AFOSR-TR- 86-1097

AD-A174 568

PSI-015/
TR-522

TURBULENT BOUNDARY LAYER HEAT TRANSFER IN HIGH SPEED FLOWS

Final Report
for the period
1 November 1979 - 30 September 1983

by

M. L. Finson and H. H. Legner

July 1985

Submitted to.

Air Force Office of Scientific Research
Bolling Air Force Base
Washington, DC 20332

Under Contract No. F49620-80-C-0015

PHYSICAL SCIENCES INC.
RESEARCH PARK, ANDOVER, MA 01810

86 11 25 274

REPORT DOCUMENTATION PAGE

1a. REPORT SECURITY CLASSIFICATION: UNCLASSIFIED	1b. RESTRICTIVE MARKINGS
2a. SECURITY CLASSIFICATION AUTHORITY	3. DISTRIBUTION/AVAILABILITY OF REPORT: Approved for public release; distribution unlimited.
2b. DECLASSIFICATION/DOWNGRADING SCHEDULE	
4. PERFORMING ORGANIZATION REPORT NUMBER(S): PSI-015/TR-522	5. MONITORING ORGANIZATION REPORT NUMBER(S): AFOSR-TR- 86-1097
6a. NAME OF PERFORMING ORGANIZATION: Physical Sciences Inc. — 6b. OFFICE SYMBOL (If applicable)	7a. NAME OF MONITORING ORGANIZATION: Air Force Office of Scientific Research, Director of Aerospace Sciences
6c. ADDRESS (City, State and ZIP Code): Dascomb Research Park, P.O. Box 3100, Andover, MA 01810	7b. ADDRESS (City, State and ZIP Code): Bolling AFB, DC 20332
8a. NAME OF FUNDING/SPONSORING ORGANIZATION: AFOSR — 8b. OFFICE SYMBOL (If applicable): NA	9. PROCUREMENT INSTRUMENT IDENTIFICATION NUMBER: F49620-80-C-0015
8c. ADDRESS (City, State and ZIP Code): Bldg 410, Bolling AFB DC 20332	10. SOURCE OF FUNDING NOS.

PROGRAM ELEMENT NO.	PROJECT NO.	TASK NO.	WORK UNIT NO.
[illegible]	2307	A1	

11. TITLE (Include Security Classification) Turbulent Boundary Layer Heat Transfer in High Speed Flows

12. PERSONAL AUTHOR(S) M. L. Finson and H. H. Legner

13a. TYPE OF REPORT	13b. TIME COVERED	14. DATE OF REPORT (Yr., Mo., Day)	15. PAGE COUNT
Final	FROM 11/79 TO 9/83	July 1985	

16. SUPPLEMENTARY NOTATION

17. COSATI CODES			18. SUBJECT TERMS (Continue on reverse if necessary and identify by block number)
FIELD	GROUP	SUB. GR.	

19. ABSTRACT (Continue on reverse if necessary and identify by block number)

Attempts at developing an improved engineering method for predicting separated supersoinc turbulent flows are reported. The approach is based on the use of an inverse boundary layer method, coupled with a five-equation Reynolds stress turbulence model, comparisons of results of the turbulence model with measurements on attached boundary layers in adverse boundary layers showed that the model predicts too large an increase in the turublent Reynolds stress. Most of the existing inverse boundary layer methods could not be readily applied to the present problem. A "second" approach was adopted, but proved to be not very "robust." Attempts to simulate separated flows failed to yield a proper separation zone, apparently due to excessive build-up of the Reynolds stress. Finally, it is noted that reliable algorithms for matching the boundary layer solution in the outer inviscid flow need to be developed.

20. DISTRIBUTION/AVAILABILITY OF ABSTRACT: UNCLASSIFIED/UNLIMITED ☒ SAME AS RPT. ☐ DTIC USERS ☐	21. ABSTRACT SECURITY CLASSIFICATION: UNCLASSIFIED
22a. NAME OF RESPONSIBLE INDIVIDUAL: James D. Wilson	22b. TELEPHONE NUMBER (Include Area Code): [illegible] — 22c. OFFICE SYMBOL: N A

DD FORM 1473, 83 APR — EDITION OF 1 JAN 73 IS OBSOLETE.

PSI-015/
TR-522

TURBULENT BOUNDARY LAYER HEAT TRANSFER IN HIGH SPEED FLOWS

Final Report
for the period
1 November 1979 - 30 September 1983

Under Contract No. F49620-80-C-0015

by

M. L. Finson and H. H. Legner

Submitted to:

Air Force Office of Scientific Research
Bolling Air Force Base
Washington, DC 20332

Submitted by:

PHYSICAL SCIENCES INC.
Dascomb Research Park, P.O. Box 3100
Andover, MA 01810

July 1985

TABLE OF CONTENTS

LIST OF ILLUSTRATIONS

LIST OF ILLUSTRATIONS (Continued)

1. INTRODUCTION

Flow separation introduces major complications for the designer of high-speed flight vehicles. Separation can result in increased drag, loss of lift, buffeting, reduced control surface effectiveness, and very high heating in the reattachment zone. These effects are most pronounced at high Reynolds numbers, where the boundary layer is turbulent. Computing a separated flow is, of course, a much more difficult task than computing an attached boundary layer. Modeling the turbulence behavior is the other major problem.

Separated two-dimensional (2-D) flows have been studied extensively. The more recent works have concentrated on numerical solutions to the Navier-Stokes equations. Shang and Hankey[1] used a parabolized Navier-Stokes (PNS) method for shock-separated flows; they found that a lag method is required to achieve decent agreement with observed pressure distributions in separation zones. In a series of papers, Horstman[2] and co-workers investigated several turbulence models in Navier-Stokes solutions for shock-separated flows. The turbulence models include an algebraic eddy viscosity model, a one-equation model consisting of an additional partial differential equation for the turbulent kinetic energy, and a two-equation model (pde's for turbulent kinetic energy and length scale). They found that the more sophisticated models (i.e., the one- and two-equation turbulence models) yield somewhat better agreement with detailed measurements of shock-separated flows. However, none of the models were entirely satisfactory.

This report summarizes the results of a study to develop an improved engineering method for predicting separated supersonic turbulent flows. The approach is based on the use of an <u>inverse boundary layer</u> method, coupled with a five-equation Reynolds stress turbulence model. The inverse method promises to permit meaningful solutions to the boundary layer equations for separated flows, with much less numerical effort than would be required to solve the Navier-Stokes equations. The Reynolds stress modeling should be able to account for the important effects of adverse pressure gradients. Pressure

gradients significantly alter the distribution of energy between turbulence components, an effect that is not readily incorporated into simpler one- or two-equation models. The goal, then, is to obtain an accurate description of turbulence behavior in supersonic separated flows, at a computational effort appropriate to engineering applications.

All of the discussion here will be restricted to 2-D separated flows. Three-dimensional separation may be more important for real applications, and the 2-D idealization may represent a singular limit to the more general 3-D situation. Nevertheless, there is good experimental data on 2-D separation and it seems appropriate to attempt to understand the simpler case first. As will be discussed, there are several unresolved challenges to the 2-D case.

2. SECOND-ORDER CLOSURE MODEL

The development of the model used in this study has been described in detail elsewhere,[3,4] and only the results shall be presented here. Our treatment of closure draws upon aspects of various previous work, most notably Rotta's treatment of low Reynolds number effects[5] and the description by Hanjalic and Launder[6] of the triple fluctuation and pressure fluctuation terms. Wherever possible, closure approximations have been evaluated against basic laboratory experiments (e.g., grid turbulence), the types of experiments being chosen to attempt to isolate individual terms.

The formulation accounts for both mean and fluctuating velocity and temperature quantities. The dependent velocity variables are the mean velocity vector U_i, the Reynolds stress tensor $\overline{u_i'u_j'}$, and the isotropic dissipation rate Φ; under the boundary layer approximation, this set of variables reduces to $U, V, \overline{u'^2}$, $\overline{v'^2}$, $\overline{w'^2}$, $\overline{u'v'}$, and Φ. In practice, it is convenient to replace $\overline{u'^2}$, $\overline{v'^2}$, $\overline{w'^2}$ by the kinetic energy $q^2 = (\overline{u'^2} + \overline{v'^2} + \overline{w'^2})/2$ and two measures of the degree of anisotropy $S_{11} = \overline{u'^2} - 2/3\ q^2$, $S_{22} = \overline{v'^2} - 2/3\ q^2$.

For steady flow, the governing equations include continuity:

$$\frac{\partial}{\partial x_i}(\rho U_i) = 0 \tag{1}$$

the mean momentum equation:

$$\rho U_k \frac{\partial U}{\partial x_k} = -\frac{\partial \bar{p}}{\partial x} - \frac{\partial}{\partial y}\left(\rho \overline{u'v'}\right) + \frac{\partial}{\partial y}\left(\mu \frac{\partial U}{\partial y}\right) \tag{2}$$

and, for the five second-order quantities:

$$\rho U_k \frac{\partial q^2}{\partial x_k} = -\rho\overline{u'v'}\ \frac{\partial U}{\partial y} - \rho\Phi + 0.15\ \frac{\partial}{\partial y}\left[\rho\ \frac{q^2 v'^2}{\Phi}\ \frac{\partial}{\partial y}\left(q^2 + v'^2\right)\right]$$
$$+ \frac{\partial}{\partial y}\ \mu\ \frac{\partial q^2}{\partial y} + \left(S_{22} - S_{11}\right)\ \rho\ \frac{\partial U}{\partial x} \tag{3}$$

$$\rho U_k \frac{\partial S_{11}}{\partial x_k} = -\frac{14}{33}\rho\overline{uv}\frac{\partial U}{\partial y} - C_E\rho\frac{\Phi}{q^2}S_{11} + 0.15\frac{\partial}{\partial y}\left[\rho\frac{q^2v^2}{\Phi}\frac{\partial}{\partial y}\left(S_{11}-\frac{2}{3}v^2\right)\right]$$

$$+\frac{\partial}{\partial y}\mu\frac{\partial S_{11}}{\partial y} - \rho\left[\frac{8}{15}q^2+\frac{2}{33}S_{11}+\frac{1}{33}S_{22}\right]\frac{\partial U}{\partial x} \tag{4}$$

$$\rho U_k \frac{\partial S_{22}}{\partial x_k} = \frac{13}{33}\rho\overline{uv}\frac{\partial U}{\partial y} - C_E\rho\frac{\Phi}{q^2}S_{22} + 0.15\frac{\partial}{\partial y}\left[\rho\frac{q^2v^2}{\Phi}\frac{\partial}{\partial y}\left(S_{22}-\frac{4}{3}v^2\right)\right]$$

$$+\frac{\partial}{\partial y}\mu\frac{\partial S_{22}}{\partial y} + \rho\left[\frac{8}{15}q^2+\frac{1}{33}S_{11}+\frac{2}{33}S_{22}\right]\frac{\partial U}{\partial x} \tag{5}$$

$$\rho U_k \frac{\partial \overline{uv}}{\partial x_k} = -\rho\left[\frac{4}{15}q^2-\frac{2}{11}S_{11}+\frac{5}{22}S_{22}\right]\frac{\partial U}{\partial y} - C_E\rho\frac{\Phi}{q^2}\overline{uv}$$

$$+0.30\frac{\partial}{\partial y}\left[\rho\frac{q^2v^2}{\Phi}\frac{\partial\overline{uv}}{\partial y}\right]+\frac{\partial}{\partial y}\mu\frac{\partial\overline{uv}}{\partial y} \tag{6}$$

$$\rho U_k \frac{\partial \Phi}{\partial x_k} = 1.25\rho\frac{\overline{uv}}{q^2}\frac{\partial U}{\partial y}\Phi - C_\Phi\rho\frac{\Phi^2}{q^2} + 14.8\rho\frac{\nu q^2}{\Phi y^2}$$

$$+0.15\frac{\partial}{\partial y}\left[\rho\frac{q^2v^2}{\Phi}\frac{\partial\Phi}{\partial y}\right]+\frac{\partial}{\partial y}\mu\frac{\partial\Phi}{\partial y} - 1.25\rho\frac{u^2}{q^2}\frac{\partial U}{\partial x}\Phi \tag{7}$$

where $C_E = \dfrac{1.2 + 12.5\ \pi/Re_\Lambda}{1 + 12.5\ \pi/Re_\Lambda}$, $C_\Phi \dfrac{0.288 + 6.6\ \pi/Re_\Lambda + 35\ \pi^2/Re_\Lambda{}^2}{(0.4 + 5\ \pi/Re_\Lambda)^2}$

and Re is the turbulent Reynolds number q /ν, with being related to the dissipation rate by

$$\Phi = 0.4 \frac{q^3}{} + 5\pi\nu \frac{q^2}{2} = 0.4 \frac{q^3}{}\left(1 + 12.5\ \pi/\mathrm{Re}\right) \tag{8}$$

It may be noted that, in the limit Re → ∞, Eqs. (1) through (7) are somewhat similar to those derived by Launder et al.[6 7] However, low Reynolds number effects are also included here, in the molecular diffusion terms and in the Re dependence of the sink terms involving C_E and C_Φ. The term $14.8\ \rho\nu q^2/(\Phi y^2)$ is a "wall term," required to obtain a well-behaved solution in the viscous sublayer, y → 0.

For the high-speed flows, it is also necessary to describe the temperature or enthalpy field. The mean temperature is required to determine density and the Reynolds heat flux $\overline{v'T'}$ is of primary interest for heat transfer considerations. To accomplish this, we include as additional dependent variables the mean static enthalpy $\bar{h}$, the mean-square fluctuating enthalpy $\overline{h'^2}$, and the transverse and axial components of the Reynolds heat flux $\overline{v'h'}$ and $\overline{u'h'}$. Required closure approximations have been carried out in a manner analogous to those leading to the velocity equations above, although the paucity of measurements of fluctuating temperatures has made it difficult to completely verify closure approximations against basic laboratory data. The resulting ·thalpy equations are:

$$\rho \frac{D\bar{h}}{Dt} = \bar{U}\frac{\partial\bar{p}}{\partial x} - \frac{\partial}{\partial y}\left(\rho\overline{v'h'}\right) + \frac{1}{Pr}\frac{\partial}{\partial y}\left(\mu\frac{\partial\bar{h}}{\partial y}\right) + \mu\left(\frac{\partial U}{\partial y}\right)^2 + \rho\Phi \tag{9}$$

$$\rho\frac{D\overline{h'^2}}{Dt} = -2\rho\,\overline{v'h'}\frac{\partial\bar{h}}{\partial y} - C_{T_1}\,\rho\frac{\Phi}{q^2}\overline{h'^2} + 0.40\frac{\partial}{\partial y}\left(\rho\frac{q^2v^2}{\Phi}\frac{\partial\overline{h'^2}}{\partial y}\right)$$
$$+ \frac{1}{Pr}\frac{\partial}{\partial y}\left(\mu\frac{\partial\overline{h'^2}}{\partial y}\right) \tag{10}$$

$$\rho \frac{D\overline{v'h'}}{Dt} = \rho v^2 \frac{\partial \bar{h}}{\partial y} + 0.09835\ \bar{\rho}\ \overline{u'h'} \frac{\partial U}{\partial y} - C_{T_2}\ \rho \frac{\Phi}{q^2} \overline{v'h'}$$

$$+ 0.80 \frac{\partial}{\partial y}\left(\rho \frac{q^2 v^2}{\Phi} \frac{\partial \overline{v'h'}}{\partial y}\right) + \frac{1}{Pr} \frac{\partial}{\partial y}\left(\mu \frac{\partial \overline{v'h'}}{\partial y}\right) \tag{11}$$

$$\rho \frac{D\overline{u'h'}}{Dt} = -\ 0.3989\ \rho \overline{v'h'} \frac{\partial U}{\partial y} - \rho \overline{uv} \frac{\partial \bar{h}}{\partial y} - C_{T_2}\ \rho \frac{\Phi}{q^2} \overline{u'h'}$$

$$+ 0.40 \frac{\partial}{\partial y}\left(\rho \frac{q^2 v^2}{\Phi} \frac{\partial \overline{u'h'}}{\partial y}\right) + \frac{1}{Pr} \frac{\partial}{\partial y}\left(\mu \frac{\partial \overline{u'h'}}{\partial y}\right) \tag{12}$$

where $C_{T_1} = \dfrac{1.32 + 7.5\ \pi/Re_\Lambda}{1 + 12.5\ \pi/Re_\Lambda}$, $C_{T_2} = \dfrac{1.165 + 12.5\ \pi/Re_\Lambda}{1 + 12.5\ \pi/Re_\Lambda}$

It should be noted that terms involving fluctuating densities (ρ') have been dropped in deriving Eqs. (1) through (12). This is generally permissible if the edge Mach number is below 4 or 5. However, if need be, the dominant effects of density fluctuations can be included by defining a generalized Reynolds stress $R_{ij} = \overline{\rho u_i u_j}/\bar{\rho} = \overline{u_i u_j} + \overline{\rho' u_i' u_j'}/\bar{\rho}$. Once this is done, the primary effect of density fluctuations is contained in a relatively unimportant diffusional term involving $\overline{\rho' v'}$, which can be related to $\overline{v'T'}$. The resulting formulation yielded good comparisons[8] with the measurements of Horstman et al.[9] in a boundary layer at $M_e = 7$.

Boundary conditions to Eqs. (1) through (12) are generally obvious: fluctuating quantities are zero at a sold wall or at the outer edge (if there is no free-stream turbulence).

3. INVERSE BOUNDARY LAYER CALCULATIONS

The inverse boundary approach offers an attractive approach for solving separated boundary layer flows. For most hypersonic flows, separation zones are relatively thin. Normal pressure variations are small, and boundary layer theory should provide a useful approximation. Reyhner and Flugge-Lotz[10] pioneered the use of boundary layer methods for separated regions, by neglecting streamwise convection terms in reverse flow zones.

The major challenge to calculating separated flows is to couple the inner, viscous solution to the outer, inviscid solution. The conventional direct boundary layer approach (pressure or edge velocity specified as a function of streamwise distance) is singular at a separation point. This singularity precludes coupling the viscous and inviscid solution. However, as originally pointed out by Catherall and and Mangler,[11] an inverse calculation (wherein the boundary layer thickness or wall shear is prescribed vs. distance) is regular at separation points. Thus, it should be possible to couple the viscous and inviscid solutions. Of course, the displacement thickness δ^* would be the appropriate boundary layer thickness to specify for this coupling process.

Wigton and Holt[12] have outlined how this coupling should be carried out. One first computes the inverse boundary layer flow given an approximate δ^* consistent with the flow configuration. Then one computes the inviscid flow past the shape that includes the same δ^*. In general, these two calculations will yield different pressure distributions. Then, based on some knowledge of the viscous and inviscid flow characteristics, a revised δ^* is selected to yield a better pressure match. The iteration continues until both viscous and inviscid solutions yield essentially the same pressure fields.

Several inverse boundary layer methods have been developed in recent years. Cebeci[13] used an inverse approach to compute attached compressible boundary layers, both laminar and turbulent, with either $c_f(x)$ or $\delta^*(x)$

prescribed. A Newton's method was used to determine the unknown edge pressure at each station, which involved inverting a matrix of derivatives of the finite-difference equations with respect to the unknown pressure. While quite sound, this matrix inversion would be cumbersome to apply to the present Reynolds stress formulation. It would be necessary to differentiate all of our equations for turbulent variables with respect to the pressure; this would greatly expand the required matrix inversion process, which is already complicated by the stiff nature of the governing equations for the Reynolds stress variables.

Cebeci, Keller, and Williams[14] (see also Cebeci and Stewartson[15]) obtained inverse boundary layer solutions of separated, incompressible laminar flows. The velocity components are transformed to the standard stream function as the dependent variable. Specification of the displacement thickness $\delta^*(x)$ yields an outer boundary condition on the stream function:

$$\Psi(x,y_e) = \rho U_e(x)(y_e - \delta^*(x)) \text{ for } y = y_e \quad . \tag{13}$$

This follows directly from the definitions of stream function and displacement thickness, and provides an additional boundary condition to the usual ones ($U=V=0$ at $y=0$, $U=U_e$ at $y=y_e$). Thus the boundary conditions are overspecified, and the edge velocity $U_e(x)$ is obtained as an eigenvalue. Cebeci, Keller and Williams showed good agreement with earlier results of Carter (to be discussed shortly), with far fewer iterations than required by Carter's methods.

While quite sound, the Cebeci, Keller and Williams method is not easily extended to compressible flows. Equation (13) still holds, with ρ replaced by $\rho_e(x)$. But, use of the streamfunction as the dependent variable results in the appearance of partial derivatives of the density in the momentum equation. These derivatives could be eliminated by use of a density-transformed y coordinate

$$Y = \int_o^y \frac{\rho}{\rho_e} dy \tag{14}$$

but then it would be necessary to perform an integral to obtain y_e in Eq. (13):

$$y_e = \int_0^{Y_e} \frac{\rho}{\rho_e}\, dY \quad . \tag{15}$$

Such terms involving density variations are quite significant in hypersonic flows, where the density can vary by large factors across the boundary layer or in the streamwise distance. Of course, an energy equation must be solved simultaneously, which provides the required thermodynamic information to determine the density. However, the density variations make it difficult to apply the inverse calculations with this method. For example, suppose the integral of Eq. (15) is inserted in Eq. (13) for y_e. The variation of the integral of $\int \rho^{-1}\, dY$ with downstream distance can be as large as changes in δ^*, at least over certain regions. This makes it very difficult in practice to obtain reliable, accurate inverse solutions for high-speed flows with such an approach.

In a series of papers, Carter (see Ref. 16) has pursued a somewhat different approach to inverse calculations, which he has successfully extended to compressible laminar and turbulent (with an eddy viscosity model) applications. Carter uses the density-transformed normal coordinate (Eq. (14)) and the standard streamfunction

$$\frac{\partial \Psi}{\partial y} = \rho U ; \quad \frac{\partial \Psi}{\partial x} = -\rho V \quad . \tag{16}$$

With these definitions, the convective operator becomes

$$\rho U \frac{\partial}{\partial x} + \rho V \frac{\partial}{\partial y} = \rho_e U \frac{\partial}{\partial x} - \frac{\partial \Psi}{\partial x}\frac{\partial}{\partial Y} \quad . \tag{17}$$

Carter then introduces a perturbation streamfunction:

$$\hat{\Psi} = \Psi - \rho_e U\left[\int_0^{Y_e} \frac{\rho_e}{\rho}\, dY - \delta^*\right] \tag{18}$$

or, rearranging,

$$\hat{\Psi} = \Psi - \rho_e U\delta^*(\eta - 1 + t^*) \tag{19}$$

$$\eta = Y/\delta^*, \quad t^* = \int_0^\infty \left(\frac{\rho_e}{\rho} - 1\right) d\eta \quad .$$

The perturbation streamfunction obeys the following differential equation:

$$\frac{\partial\hat{\Psi}}{\partial\eta} = -\rho_e U_e \delta^*(\eta - 1 + t^*) \frac{\partial(U/U_e)}{\partial\eta} \tag{20}$$

and satisfies the outer boundary condition

$$\hat{\Psi} \to 0 \quad \text{as} \quad \eta \to \infty \quad . \tag{21}$$

The major advantage of the perturbation streamfunction is that the prescribed displacement thickness $\delta^*(x)$ is automatically achieved; this may be seen by comparing Eqs. (18) and (21) with Eqs. (13) and (15) above. Thus the specified boundary layer growth is basically satisfied through a boundary condition (Eq. (21)), at the expense of an additional first-order partial differential equation (Eq. (20)). Also, Eq. (17) requires $\partial\Psi/\partial x$, which may be related to $\hat{\Psi}$ and δ^* through Eq. (19).

In the initial stages of this program, we implemented Carter's method for laminar boundary layers and reproduced some of his earlier results. Figures 1 and 2 show calculations for a separated laminar boundary layer, compared to Carter's solution and the Navier-Stokes computation by Briley.[17] Not only was Carter's calculation reproduced, but also the good agreement with the more exact Navier-Stokes solution indicates the utility of the boundary layer approach for flows with thin separation zones.

As already mentioned, Carter extended his method to turbulent flows, using an eddy viscosity formulation. However, we found the method to be difficult to apply to the more sophisticated Reynolds stress turbulence

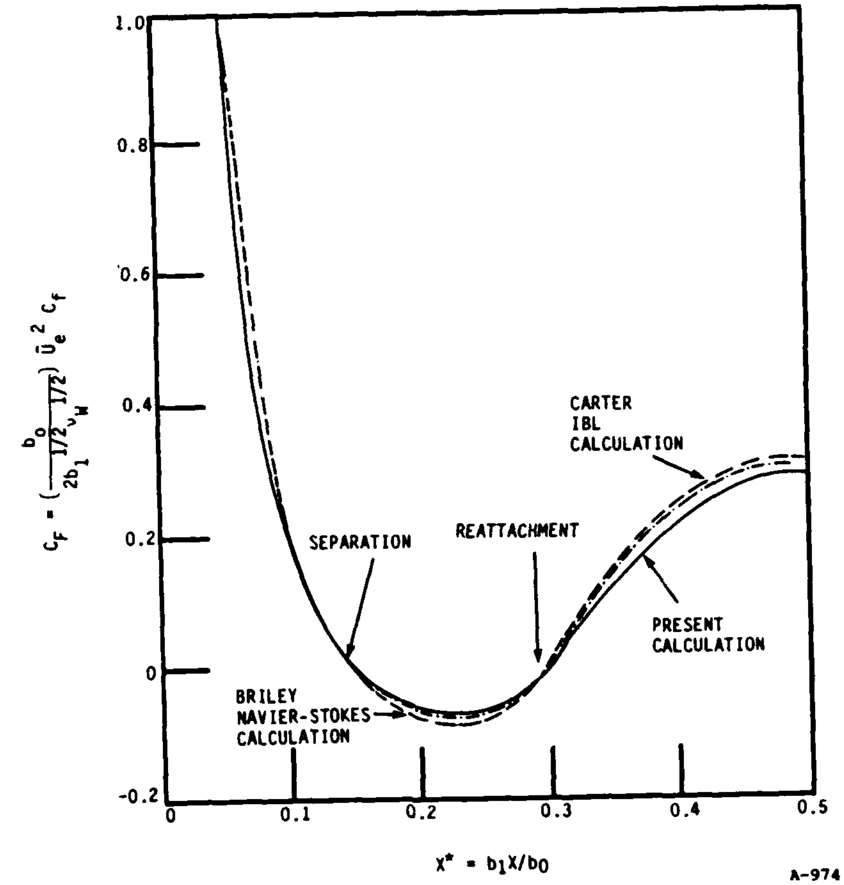

Figure 1. Skin friction variation with downstream distance for the modified Howarth problem. C_F is the normalized friction parameter used by Briley with $U_e = b_o - b_1X$.

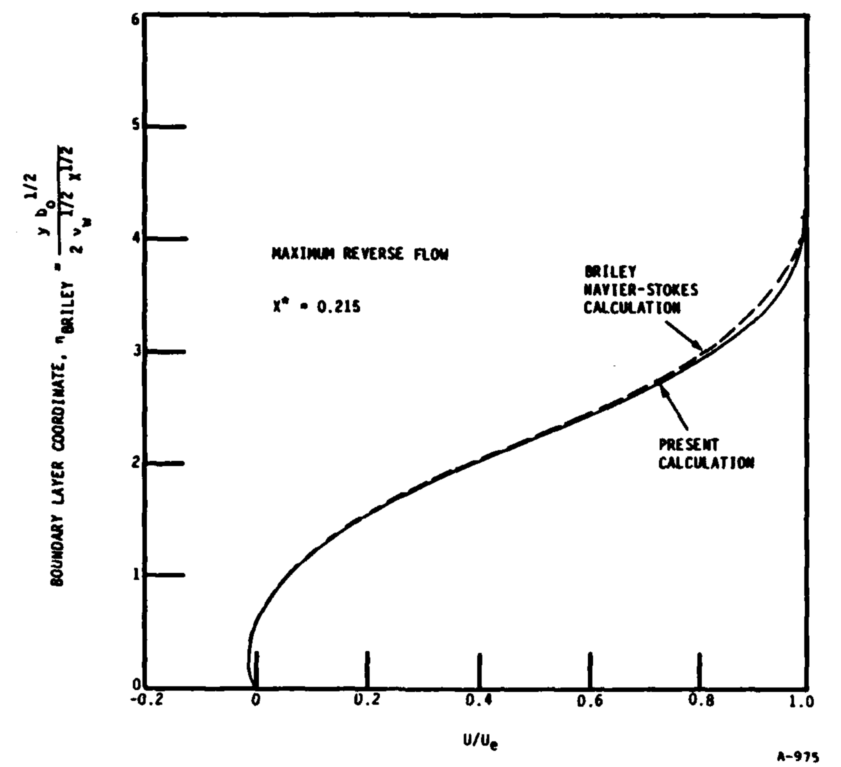

Figure 2. Velocity profile comparison at maximum reverse flow

formulation. The complications arise from some of the numerical constraints associated with the solution of the five simultaneous turbulence variables. These equations are nonlinear, strongly coupled, and often "stiff" (i.e., the right sides are dominated by production and dissipation terms, which nearly cancel).

The normal velocity convective term involves $\partial\Psi/\partial x$, which is related to the perturbation streamfunction by

$$\frac{\partial \Psi}{\partial x} = \frac{\partial \hat{\Psi}}{\partial x} + \rho_e U_e \delta^* \bar{U} \frac{dt^*}{dx} + \bar{U}\left(\eta - 1 + t^*\right) \frac{d}{dx}\left(\rho_e U_e \delta^*\right)$$

$$+ \rho_e U_e \delta^* \left(\eta - 1 + t^*\right) \frac{\partial \bar{U}}{\partial x} \quad . \tag{22}$$

In solving the Reynolds stress equation, it is frequently necessary to take very small steps in the streamwise direction. This is required for successful use of Newton's method for solving the turbulence equations. Typically, the step size Δx is chosen so that none of the dependent variables changes by more than a specified percentage (e.g., 10 or 20 percent) from one step to the next. In the start-up process, the initial step sizes are no larger than the smallest Δy values, to allow a smooth adjustment of the unknown values to their "stiff" solutions. For a high Reynolds number turbulent boundary layer, the smallest Δy in the viscous sublayer can be several orders of magnitude less than the boundary layer thickness. Of course, the step size Δx subsequently grows exponentially to reasonably large values. But, when taking small steps, the terms $\partial\hat{\Psi}/\partial x$ and $\partial\bar{U}/\partial x$ in Eq. (22) can have quite large values. Physically, $\partial\Psi/\partial x$ should be well behaved, which means that the right side of Eq. (22) can be expected to involve small differences of large numbers. Thus, with small Δx steps the convective operator, the <u>left</u> side of the governing equations, is <u>stiff</u>. We were not successful in developing a reliable numerical method for solving such a "doubly-stiff" set of equations. The difficulty does not arise if small steps are avoided, as Carter was able to do with an eddy viscosity formulation. However, the perturbation streamfunction approach implies a minimum acceptable step size, whereas the Reynolds stress equations require a maximum step size value, and these two requirements are incompatible.

A streamfunction formulation was developed to avoid the difficult numerical aspects of Carter's perturbation streamfunction, as well as the complications associated with use of the Cebeci, Keller and Williams[14] boundary condition, Eq. (13). A normalized incompressible normal coordinate is used:

$$d\eta = \frac{\rho}{\rho_e}\frac{dy}{\delta^*};\ \eta = \frac{1}{\delta^*}\int_0^y \frac{\rho}{\rho_e}\,dy \tag{23}$$

and the normal velocity is eliminated in favor of the standard streamfunction. The convective operator becomes

$$\rho U\frac{\partial}{\partial x} + \rho v\frac{\partial}{\partial y} = \rho U\frac{\partial}{\partial x} - \frac{\rho}{\rho_e}\frac{1}{\delta^*}\left(\frac{\partial \Psi}{\partial x}\right)_\eta \frac{\partial}{\partial \eta} \tag{24}$$

If the dependent variables and density are normalized by $\rho_e(x)$ and $U_e(x)$

$$\bar{U} = U/U_e(x) \tag{25}$$

$$\bar{\rho} = \rho/\rho_e(x)$$

$$\bar{q}^2 = q^2/U_e^2(x)$$

$$\bar{\Phi} = \Phi/U_e^3(x)$$

etc.

then the governing equations for velocity and turbulent kinetic energy take the following form

$$\bar{U}\frac{\partial \bar{U}}{\partial x} = \frac{1}{\rho_e U_e \delta^*}\frac{\partial \Psi}{\partial x} + \frac{1}{\rho_e U_e \delta^*}\frac{\partial}{\partial \eta}\left(\bar{\rho}\mu\frac{\partial \bar{U}}{\partial \eta}\right) - \frac{1}{\delta^*}\frac{\partial}{\partial \eta}\left(\bar{\rho}\,\overline{u'v'}\right)$$
$$+ \frac{1}{U_e}\frac{dU_e}{dx}\left(\frac{1}{\bar{\rho}} - \bar{U}^2\right) \tag{26}$$

$$\bar{U}\,\frac{\partial \bar{q^2}}{\partial x} = \frac{1}{\rho_e U_e \delta^*}\,\frac{\partial \Psi}{\partial \eta}\,\frac{\partial q^2}{\partial \eta} - \bar{\rho}\,\overline{u'v'}\,\frac{1}{\delta^*}\,\frac{\partial \bar{U}}{\partial \eta} - \bar{\Phi} + \frac{1}{\rho_e U_e \delta^{*2}}\,\frac{\partial}{\partial \eta}\left(\bar{\rho}\mu\,\frac{\partial q^2}{\partial \eta}\right)$$

$$+ \frac{1}{\rho_e U_e \delta^{*2}}\,\frac{\partial}{\partial \eta}\left[\bar{\rho}^2\,\varepsilon\,\frac{\partial}{\partial \eta}\left(\bar{q^2} + \overline{v^2}\right)\right] - \frac{1}{U_e}\,\frac{du_e}{dx}\,2\bar{U}\,\overline{q^2} \quad . \tag{27}$$

The corresponding equations for the other Reynolds stress variables and for the enthalpy unknowns take similar forms. In addition, since the streamfunction is included as an unknown variable in Eqs. (26) and (27), an additional partial differential equation must be included, which is simply derived from its definition:

$$\rho_e U_e \delta^*\,\frac{\partial \Psi}{\partial \eta} = \bar{U} \tag{28}$$

$$\Psi = 0 \text{ at } \eta = 0 \quad .$$

This formulation, as explained thus far, does not provide a method for performing an inverse calculation. Both $U_e(x)$ and $\delta^*(x)$ are included as coefficients. If $\delta^*(x)$ is to be specified, then a technique must be provided for determining $U_e(x)$. To this end, a rather straightforward approach was taken, employing what is basically a <u>secant</u> method. At each new station, the solutions are obtained at successive values of U_e in an iterative fashion until the prescribed δ^* is obtained. With a secant method, two values of U_e are selected at the new (unknown) station. The governing equations are solved for each value, and the resulting δ^* values are computed. From these two values, one interpolates to a new U_e value corresponding to the desired δ^*. The equations are solved again for this new δ^*, and subsequent iterations performed until the prescribed δ^* value is achieved to an acceptable tolerance. In practice, after the first step, it is possible to retain the slope of the curve in Figure 3 from one step to the next, so as to avoid wasting two initial solutions before interpolating to the desired δ^*. Note that for very small steps when the turbulence variables are changing rapidly, δ^* and U_e

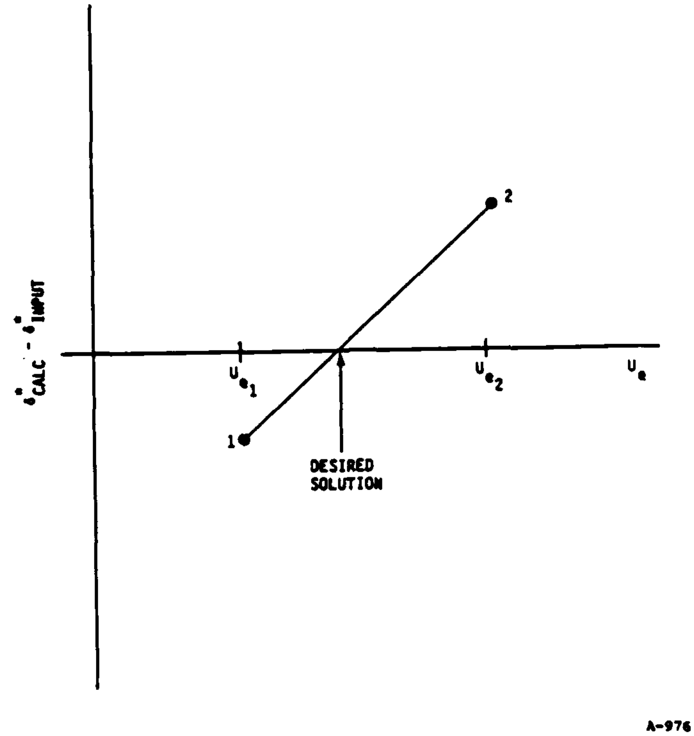

Figure 3. Sketch of secant method for inverse boundary layer solution

change only slightly from one step to the next and the secant method converges quickly. Note also that this approach is a straightforward (and perhaps less elegant) alternative to Cebeci's method.[13] In essence, he obtained the slope on Figure 3 by an elaborate matrix inversion. His technique might be more efficient numerically than that used there, but would certainly entail significantly greater analytical and programming effort.

In Figure 4 we compare the direct and inverse solutions for a Mach 7 cold wall boundary layer. The direct calculation was first performed for a flat plate, with no pressure gradient. Using the displacement thickness from this direct calculation as input, the inverse solution was then obtained according to the method just outlined. The skin friction coefficients are in good agreement, but the momentum thickness values differed by 10 to 20 percent. Of course, the displacement thickness is forced to be identical for the two calculations, so the shape factors are different. This difference undoubtedly reflects the numerical accuracy of these calculations, which involved relatively coarse grids (39 points across the boundary layer). A finer mesh appears to be necessary for accurate values of the momentum thickness.

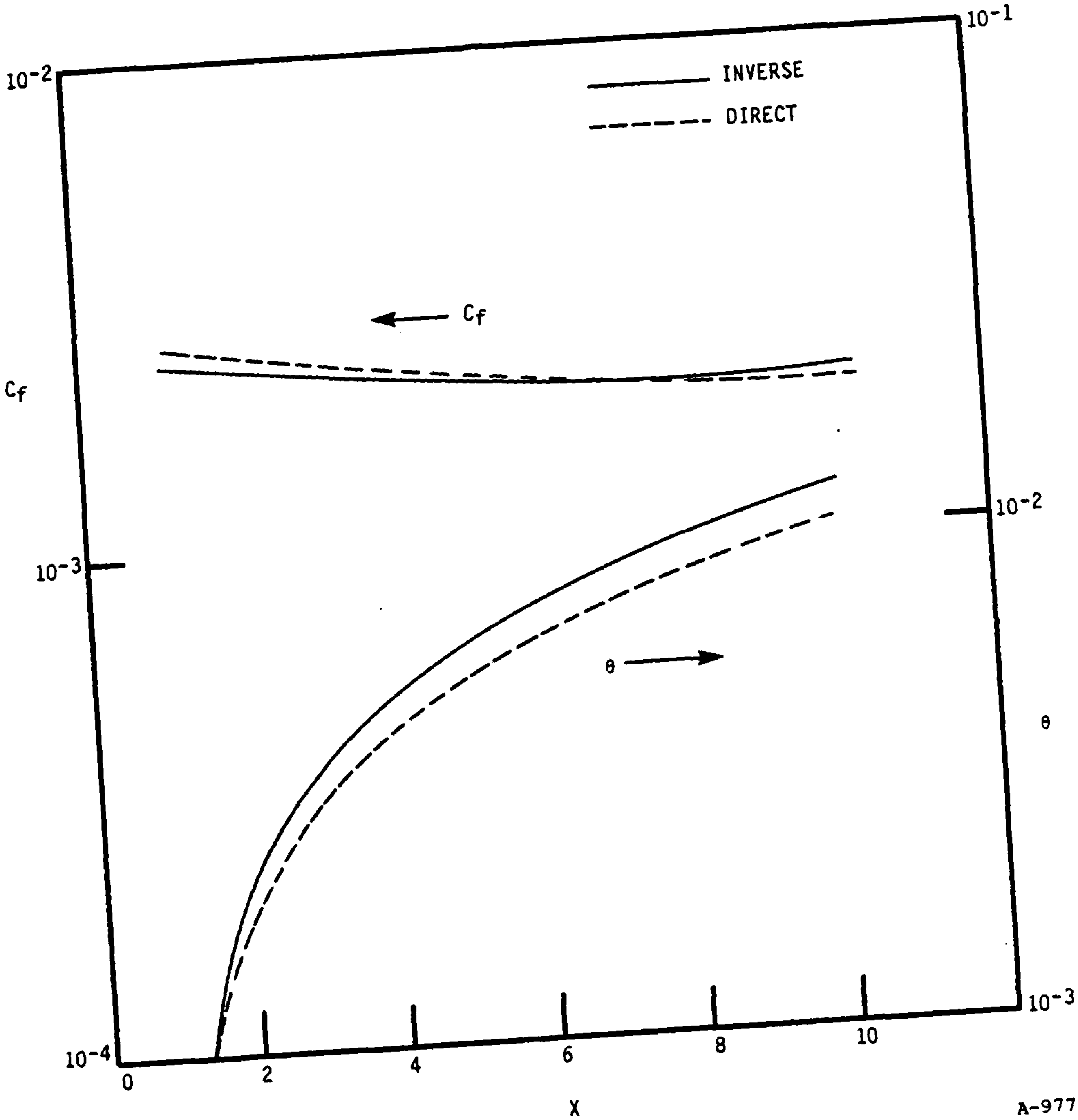

Figure 4. Comparison of direct and inverse solutions for low-speed flat plate test case

4. ADVERSE PRESSURE GRADIENTS EFFECTS

A major issue that seems particularly critical is the ability of present models to describe the detailed development of boundary layer turbulence in the presence of strong adverse pressure gradients. Pressure gradients cause significant redistributions of energy between the various components of the fluctuating turbulent energy. The "five-equation" Reynolds stress model used in this study should be superior to simpler models and, hopefully, should provide an accurate description of turbulence behavior in separating boundary layers. The closure model obeys required tensor rules, with the closure constants based on data from experiments on grid turbulence in the presence of mean shear and strain. Figure 5 is an example of a comparison between the model and measurements on grid turbulence subjected to plane strain.[18] We also examined experimental results on low-speed boundary layers in favorable pressure gradients, including the "relaminarization" effect, with reasonable success. However, in view of the importance of the turbulence behavior, we have examined several laboratory experiments on attached boundary layers in adverse pressure gradients.

Bradshaw Case C

Bradshaw's experiment[19] consisted of a low-speed boundary layer on a flat plate, artifically tripped well upstream of the region of interest. Reynolds numbers were in the range R_{e_θ} = 10,000 to 20,000, so the turbulent boundary layer should be well developed. The inviscid velocity decreased from 128 ft/sec to about 90 ft/sec over a distance of 60 in. Figure 6 shows the variation of skin friction and displacement thickness over the range of the adverse pressure gradient, and Figures 7 through 9 show the profiles of mean velocity, Reynolds stress and fluctuating velocity components at the 84 in. station, at the end of the adverse pressure gradient. The most dissappointing result is the computed Reynolds stress, which seems to be "amplified" too much by the pressure gradient. Correspondingly, the computed wall shear is high, the boundary layer becomes thicker than observed, and the mean velocity profile shape is not in detailed agreement with Bradshaw's measurements.

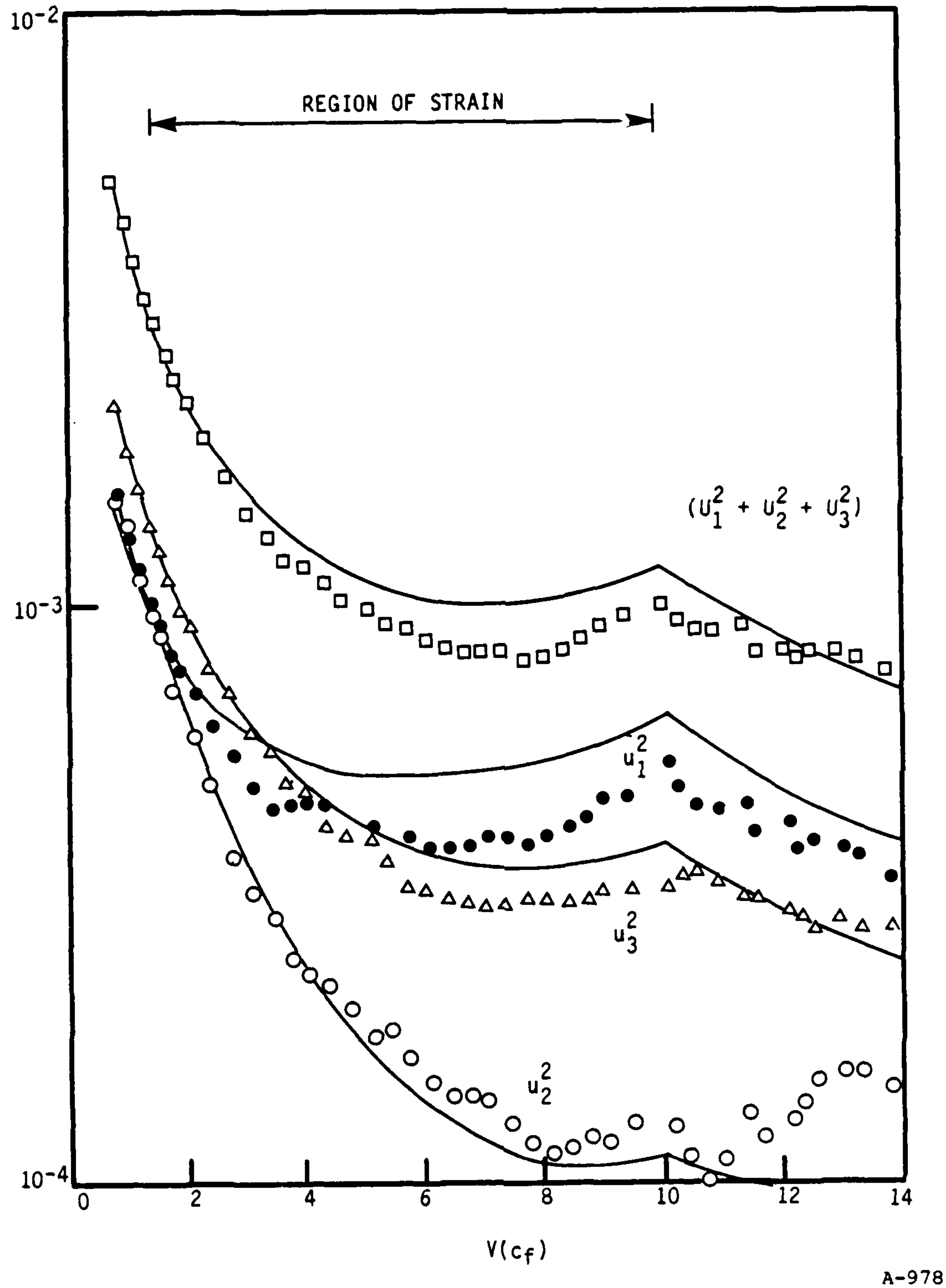

Figure 5. Decay of grid turbulence subjected to plane strain, comparisons with the experiment of Tucker and Reynolds[18]

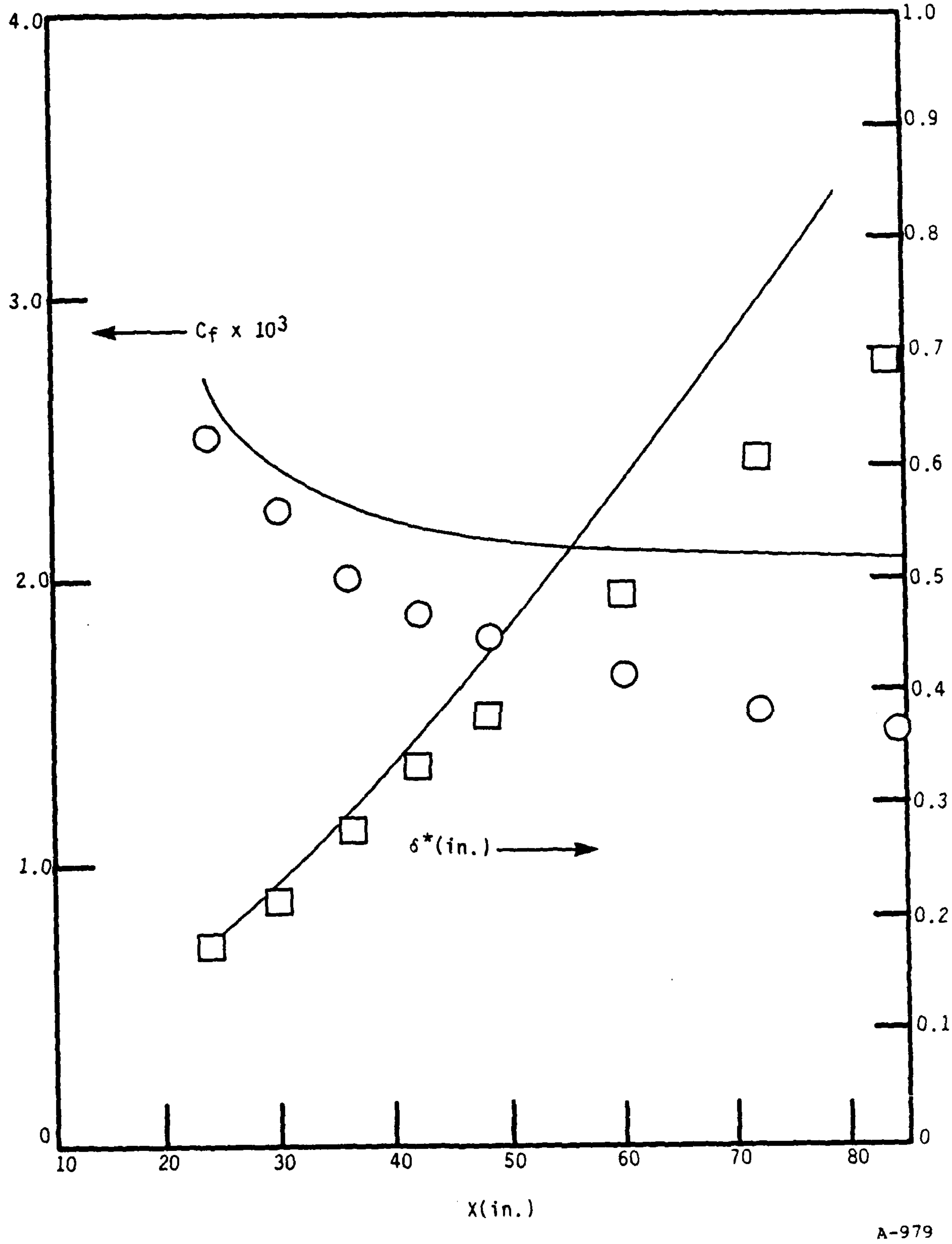

Figure 6. Comparison of computed friction coefficient and displacement thickness with measurements of Bradshaw, Case C

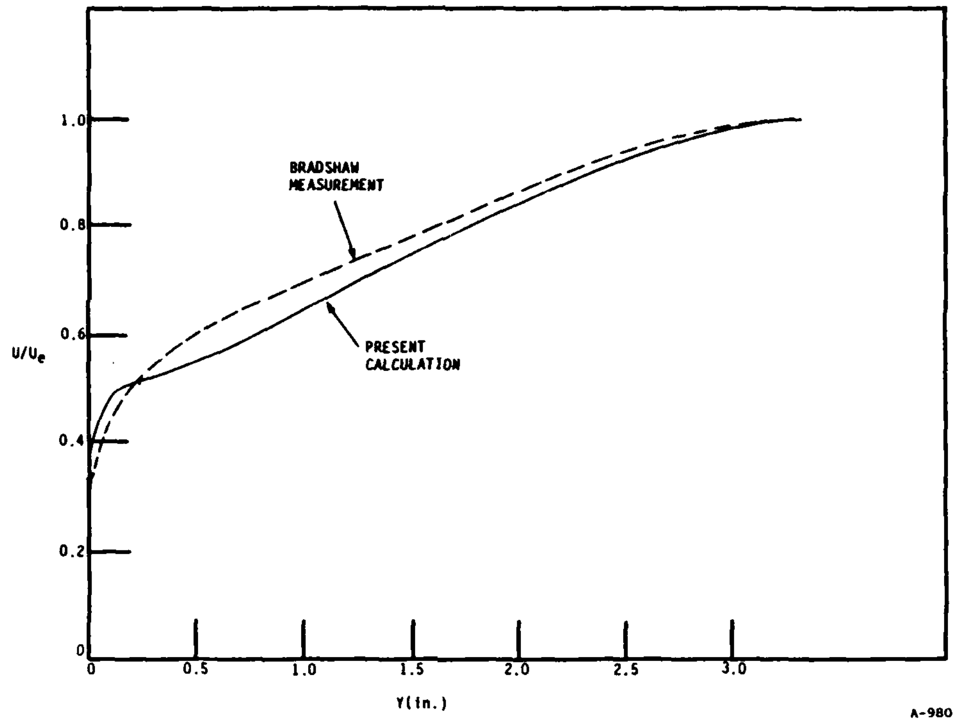

Figure 7. Comparison of computed mean velocity profile with profile measured by Bradshaw at X = 84 in.

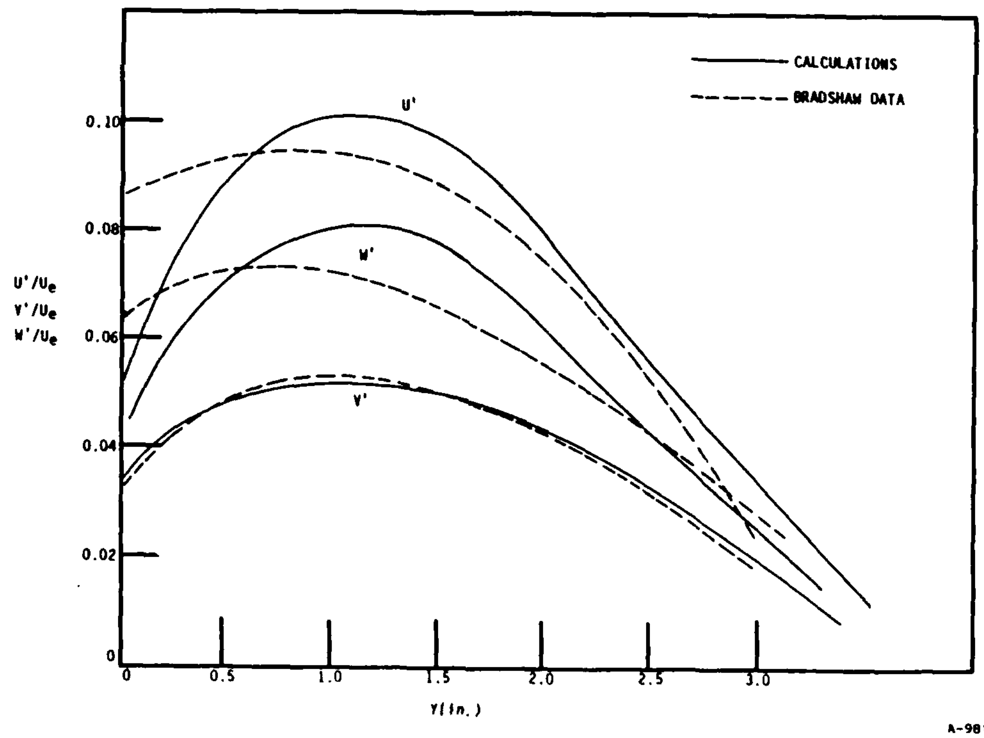

Figure 8. Comparison of computed fluctuating velocities with Bradshaw measurements at X = 84 in.

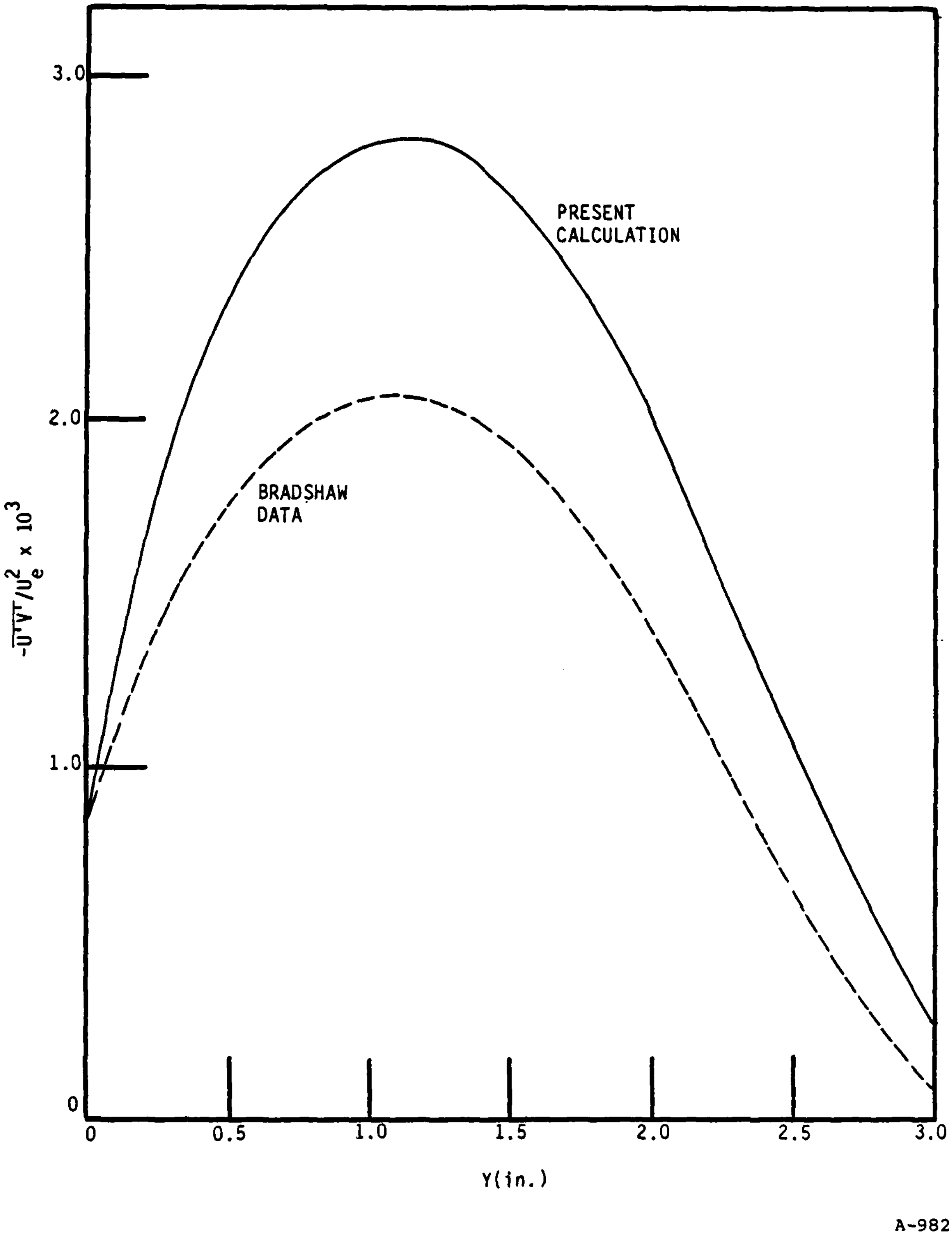

Figure 9. Comparison of computed Reynolds stress with Bradshaw measurements at X = 84 in.

Samuel and Joubert Experiment

Another experiment on an attached incompressible boundary layer in an adverse pressure was conducted by Samuel and Joubert.[20] In Figure 10 we show the variation of skin friction and displacement thickness. Profiles of mean velocity and Reynolds stress at three stations (at the onset, in the middle, and near the end of the adverse pressure gradient) are shown in Figures 11 and 12. Here again, the turbulent shear is significantly over-predicted near the end of the adverse pressure gradient. However, the computed boundary layer thickness and velocity profiles are in better agreement with the measured values.

Lewis, Gran, and Kubota

This experiment[21] involved an attached turbulent boundary layer in an adverse pressure gradient, at supersonic speeds. The boundary layer edge Mach number decreased from 4.0 to 3.0, followed by a region of favorable pressure gradient. Figures 13 through 15 show the streamwise variations of skin friction, displacement thickness and momentum thickness. In this case, in the more downstream region, the skin friction is underpredicted and the boundary layer thicknesses are overpredicted.

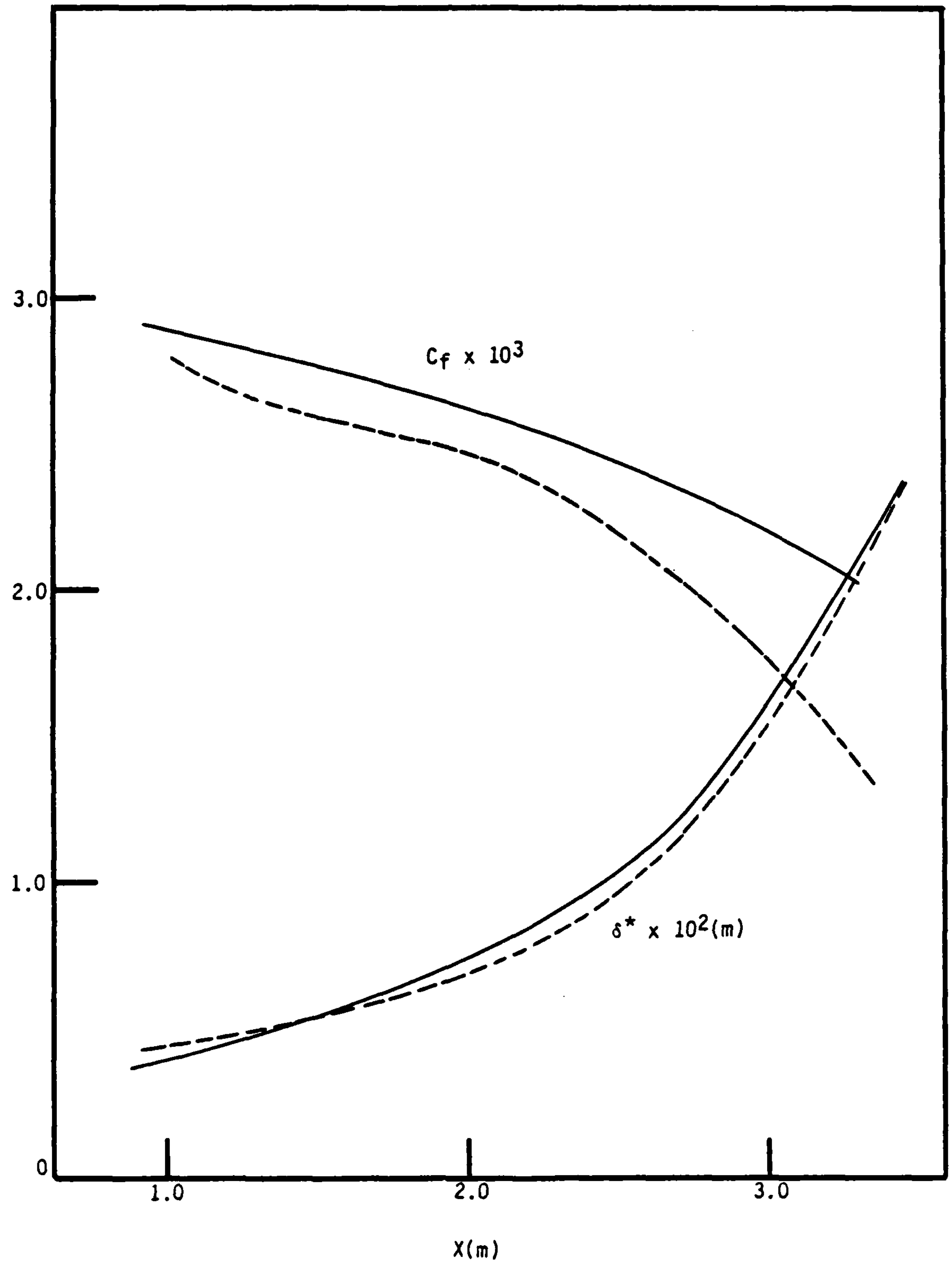

Figure 10. Comparison of computed results with measurements of Samuel and Joubert

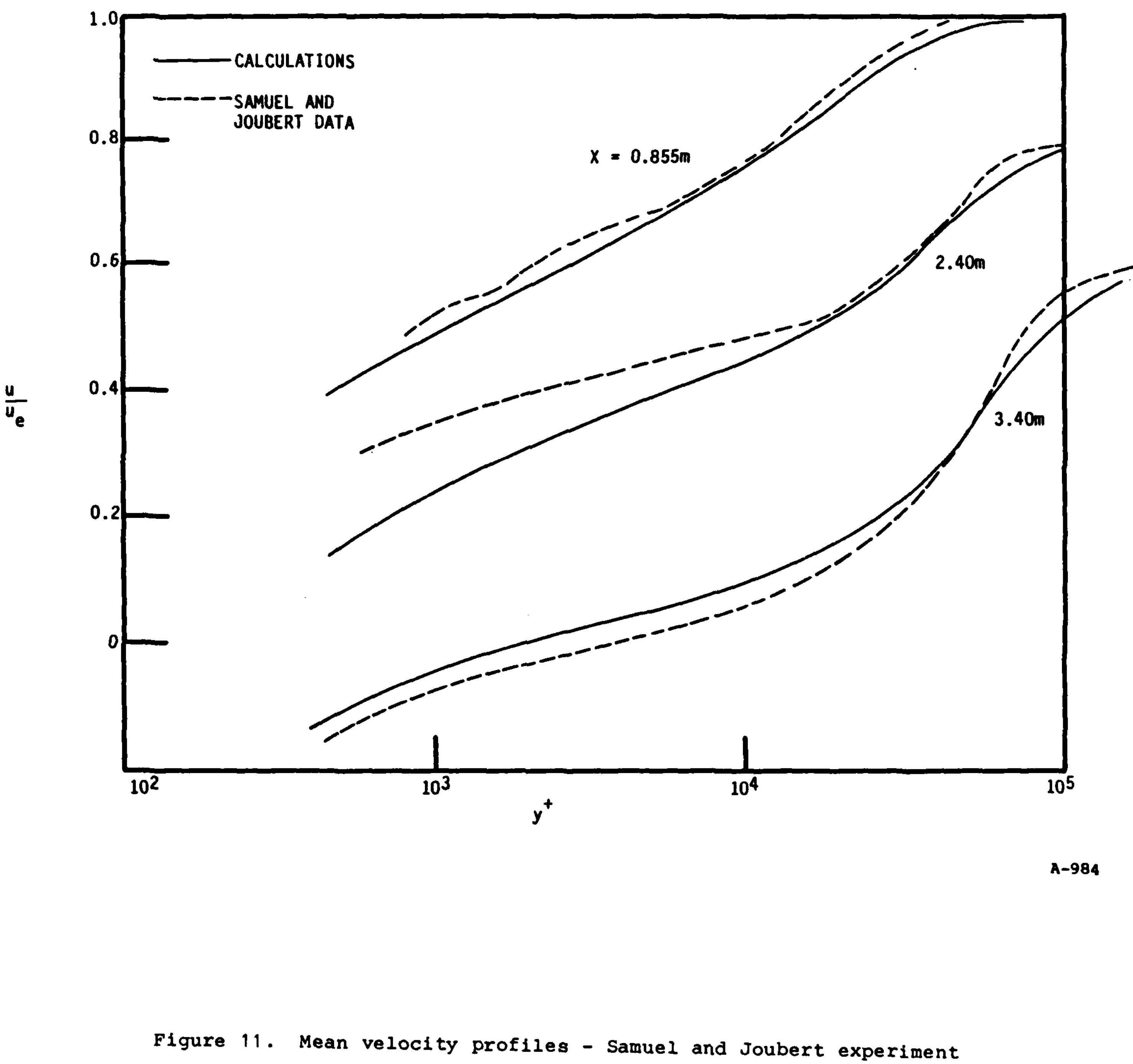

Figure 11. Mean velocity profiles - Samuel and Joubert experiment

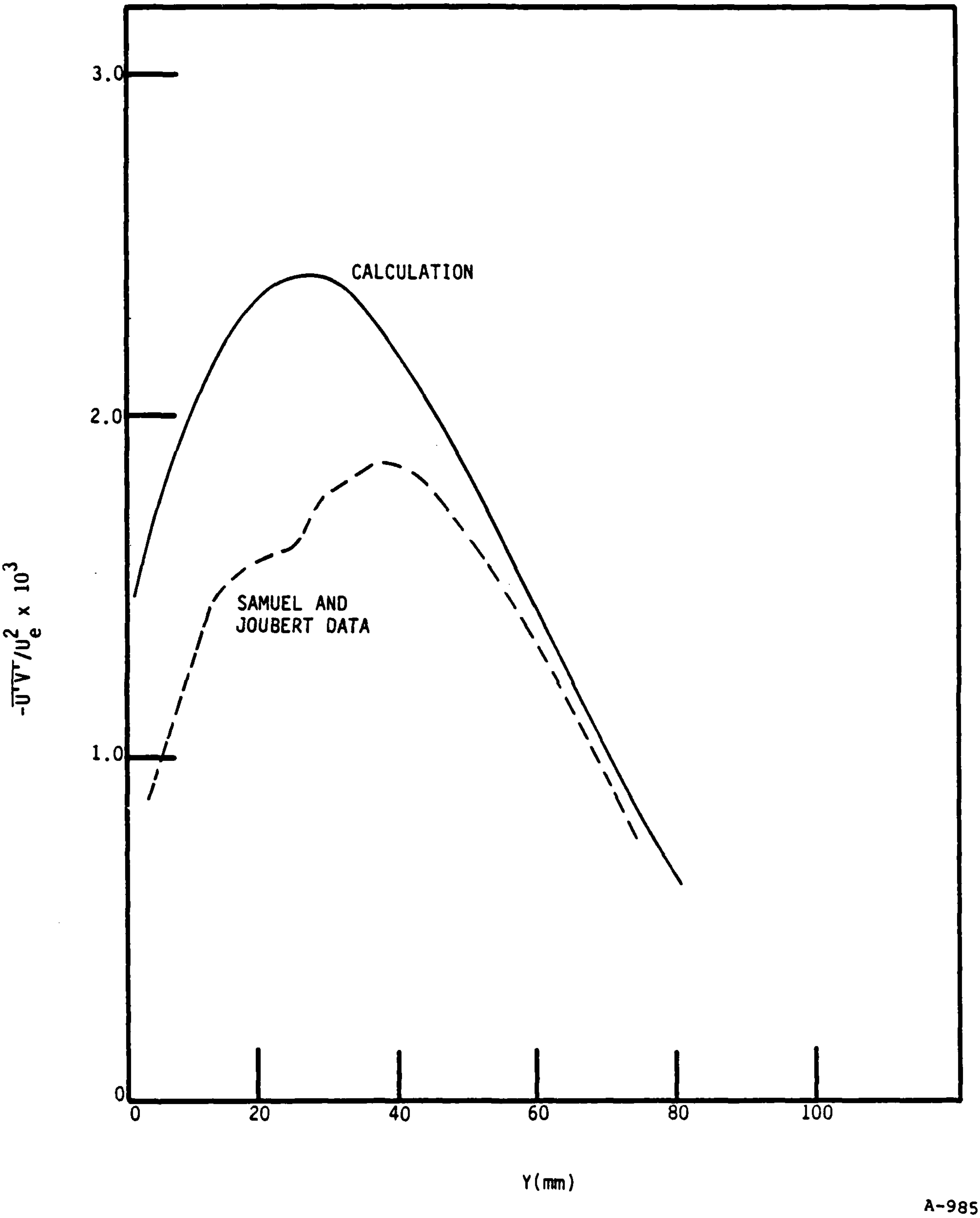

Figure 12. Reynolds stress profiles for Samuel and Joubert experiment at X = 3.4 m

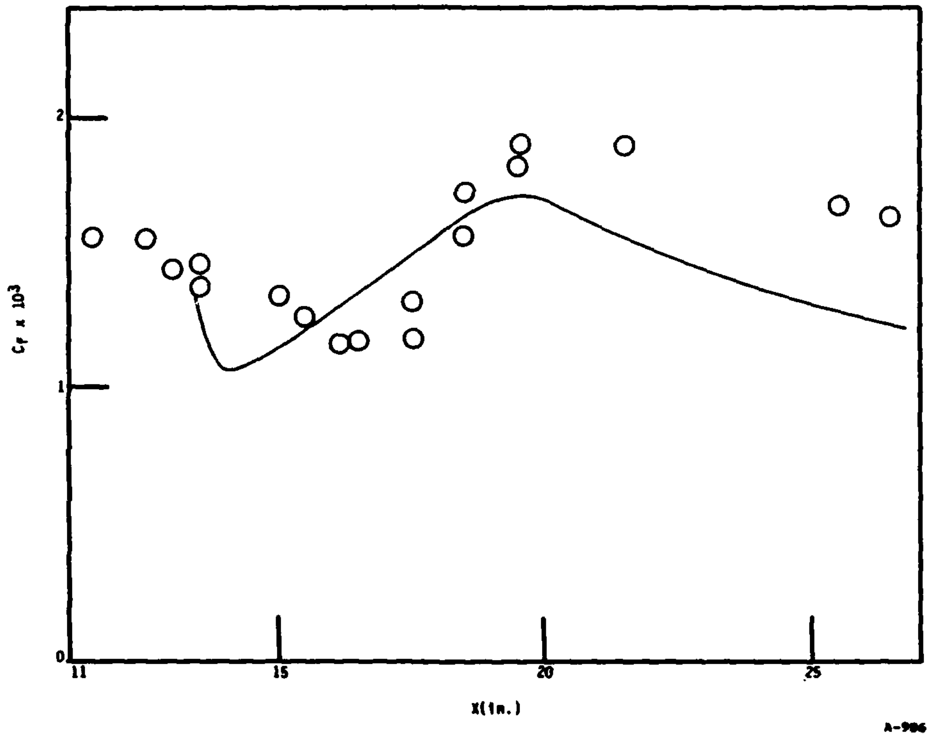

Figure 13. Skin friction coefficient comparison for Lewis, Gran, and Kubota experiment

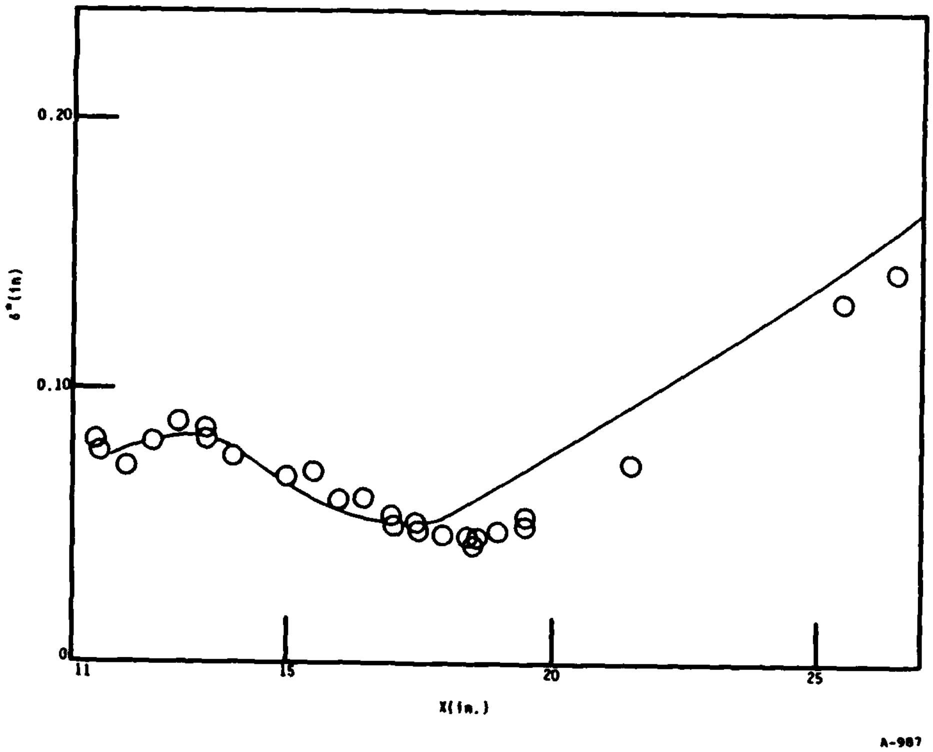

Figure 14. Displacement thickness comparison for Lewis, Gran and Kubota experiment

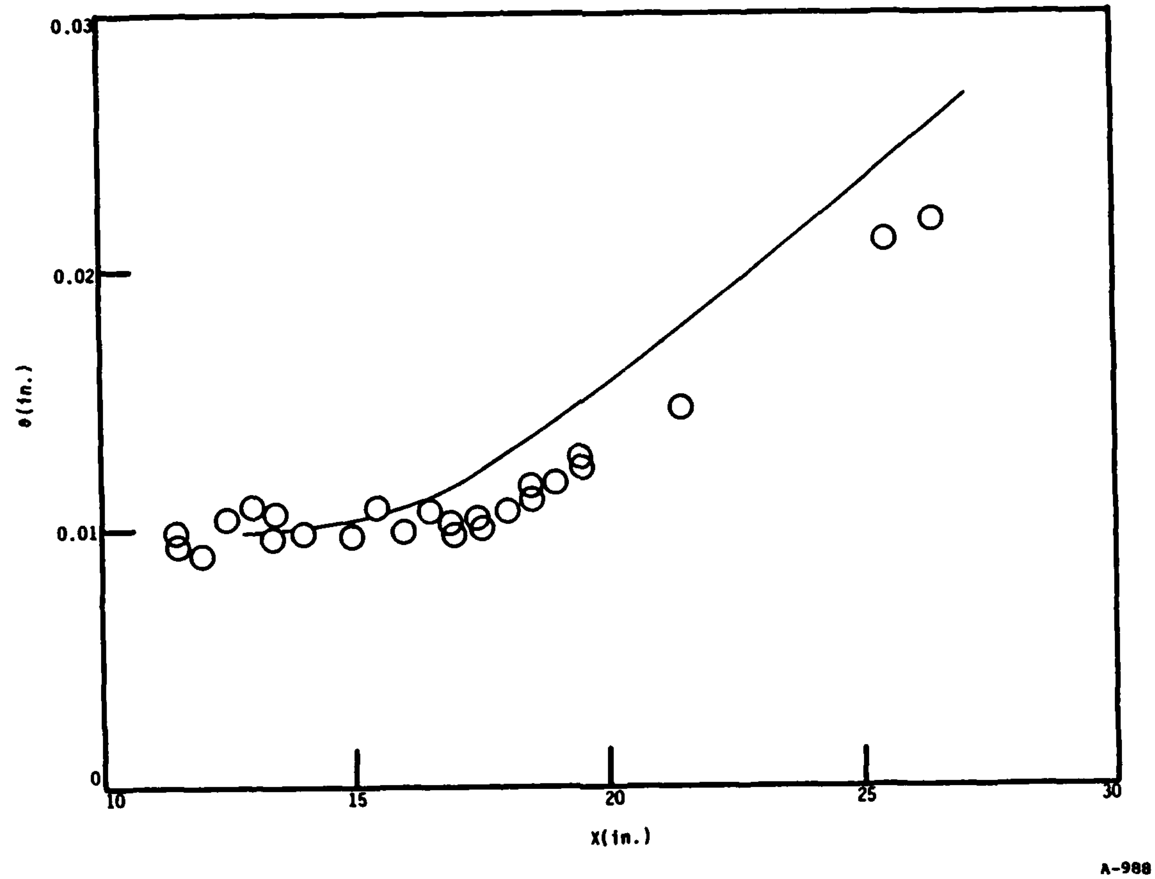

Figure 15. Momentum thickness comparison for Lewis, Green, and Kubota experiment

5. ATTEMPTS AT CALCULATING SEPARATED FLOWS

The most difficult aspect of this work, as one might expect, is the application of the inverse method to separated turbulent flows. As a first test case, we selected an incompressible, adiabatic case at a Reynolds number of 10^6, as calculated already by Carter.[16] Although no experimental data are available at the precise conditions, reproducing Carter's results with the rather different present model would seem to be a useful goal.

Carter's published displacement thickness was specified as input (Figure 16). The initial boundary layer was taken to be a classical flat plate boundary layer developed in the absence of a pressure gradient. The surprising result of our inverse calculations was that the present model does not predict separation at any point during the substantial increase of boundary layer thickness. Figure 17 shows the computed skin friction, compared to Carter's published values. Whereas the solution obtained by Carter showed separation at an X value slightly greater than 1.1, no such result occurs with our calculation. In Figure 18 we show the edge velocity derived from the solution. For the present solution, a rather more gradual adverse pressure gradient is implied.

The significant characteristic of our solution in the region where separation would be expected is the behavior of the mean velocity profile and of the Reynolds stress. Figure 19 shows the mean velocity profiles at two selected stations, along with the corresponding Reynolds stresses in Figure 20. The relative Reynolds stress is amplified by the adverse pressure gradients. At the same time, the mean velocity develops steep gradients at the wall (supporting the sustained high shear) and a "plateau" with even a mild "valley".

The mean velocity and Reynolds stress development are certainly coupled in a complex manner, and could easily be an anomolous consequence of the Reynolds stress model employed here. The development of the Reynolds stress is reminescent of the behavior in the attached adverse pressure gradient

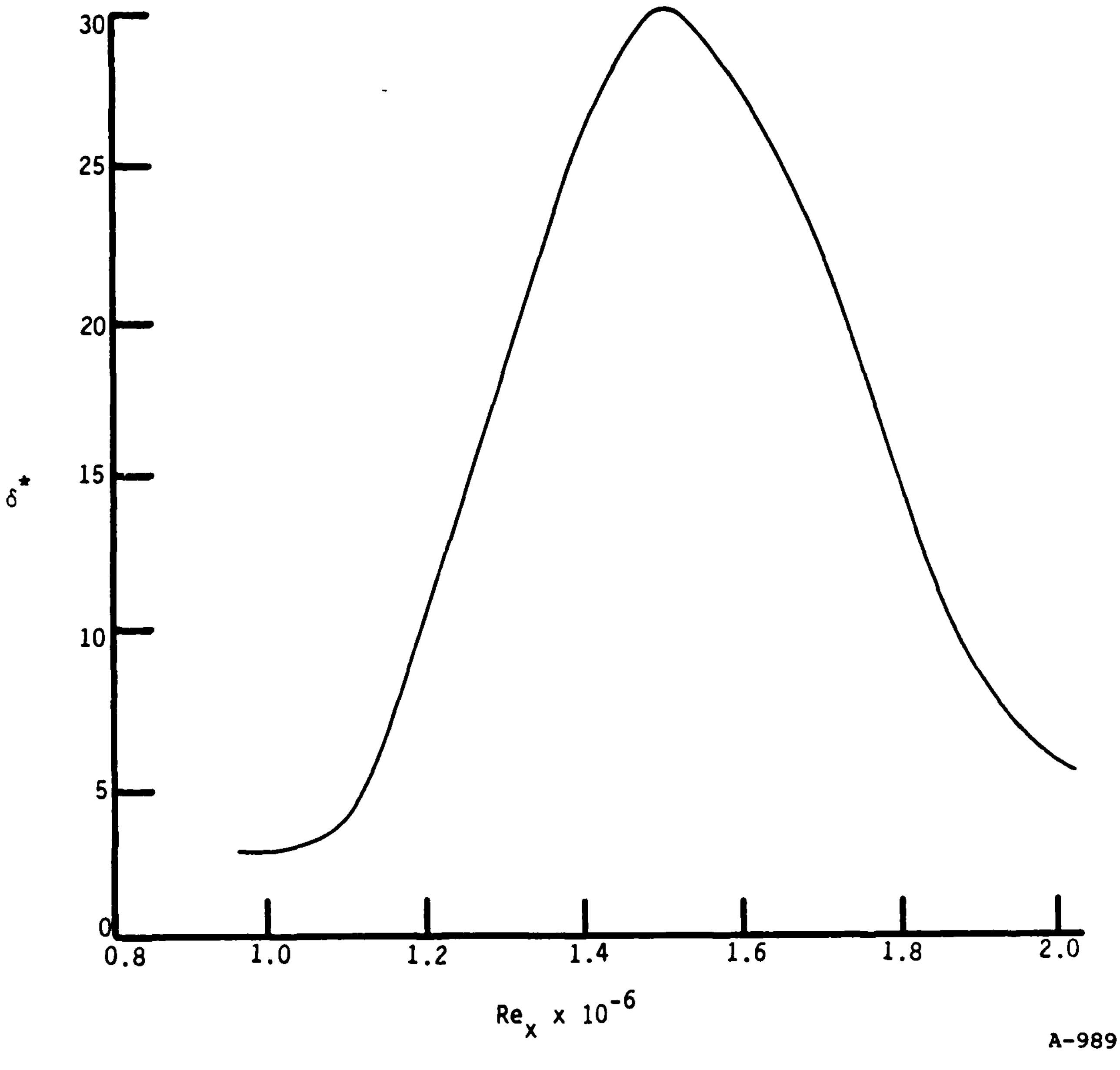

Figure 16. Input displacement thickness for Mach = 0 separated turbulent solution

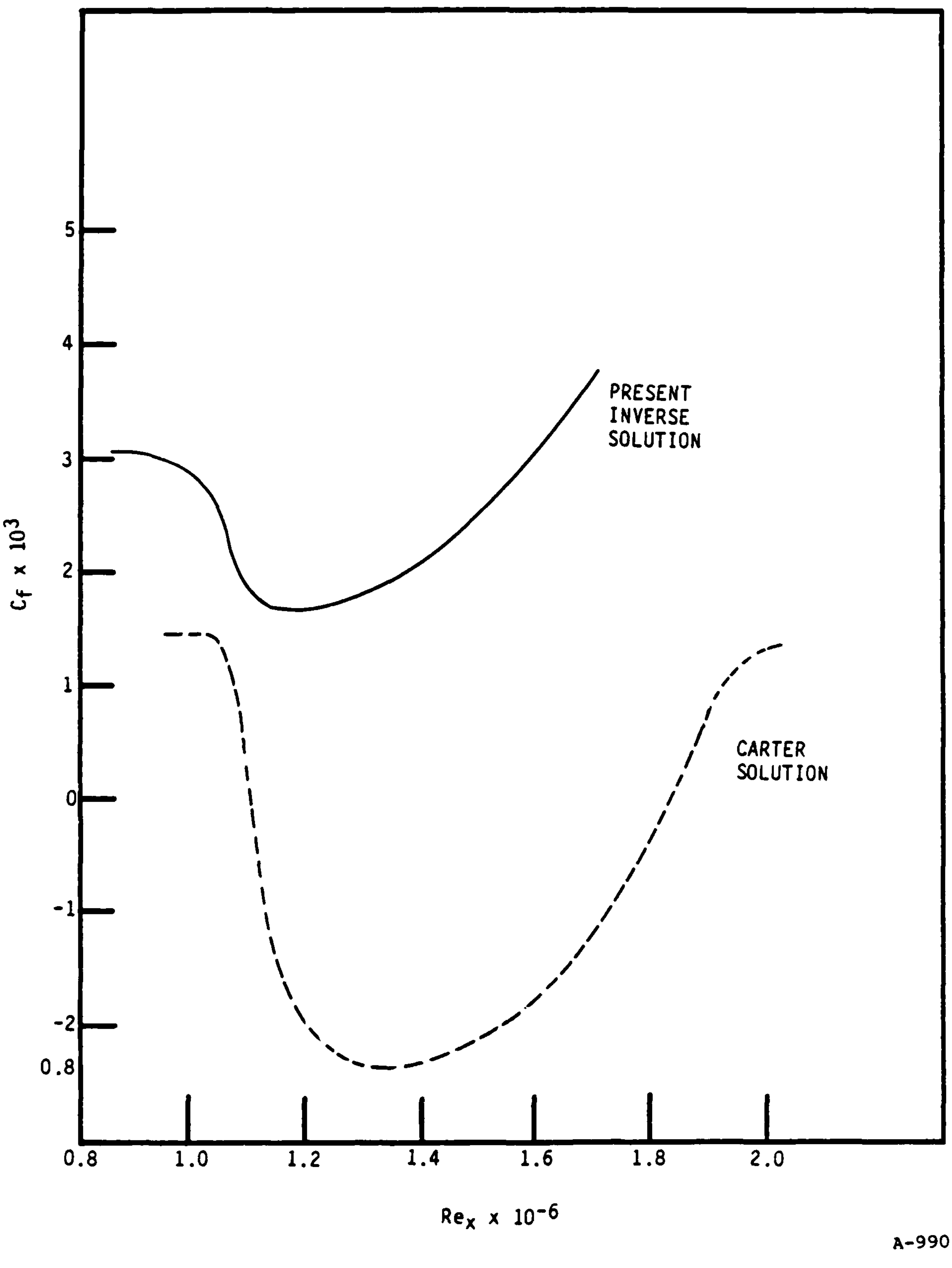

Figure 17. Skin friction solutions

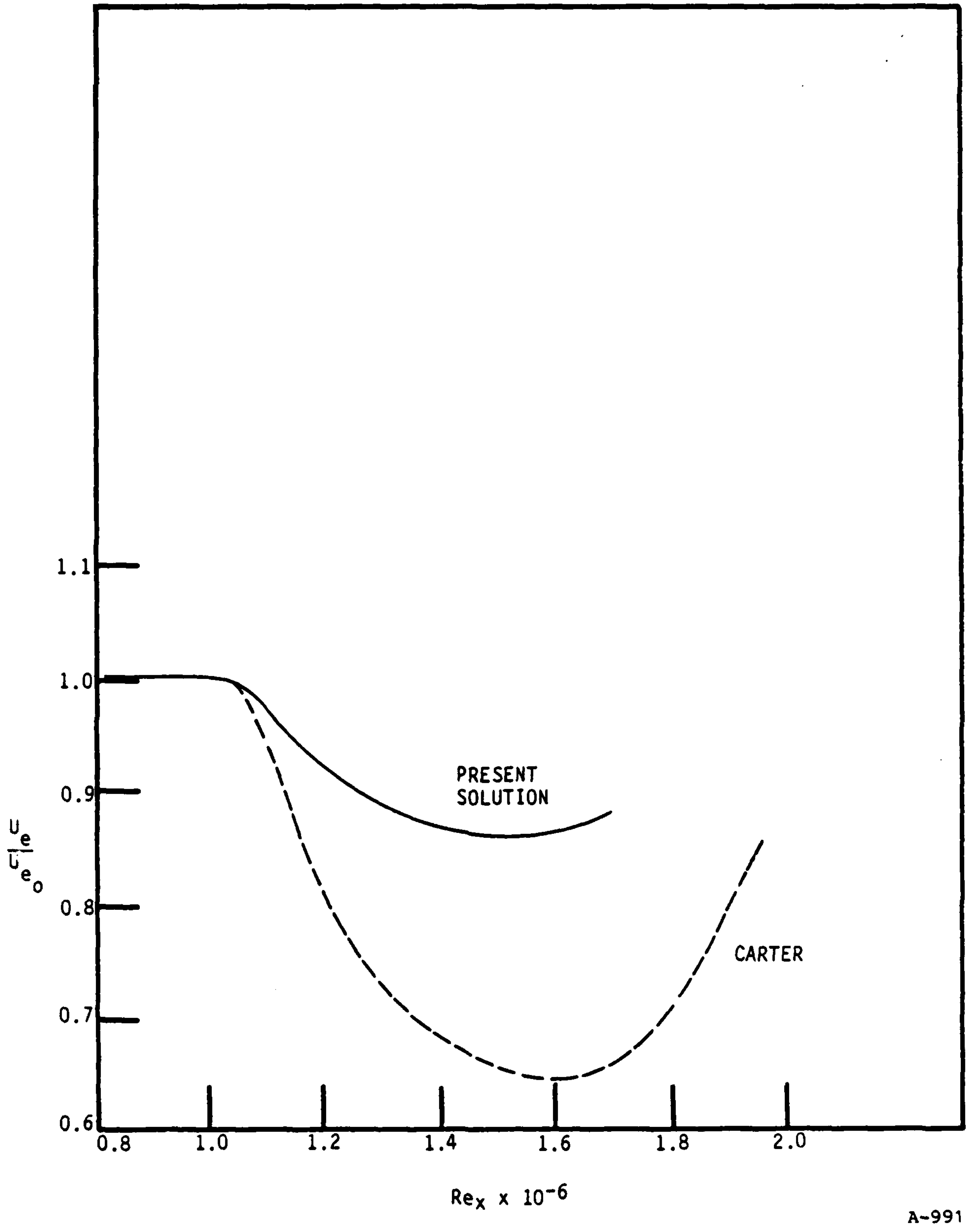

Figure 18. Computed edge velocities

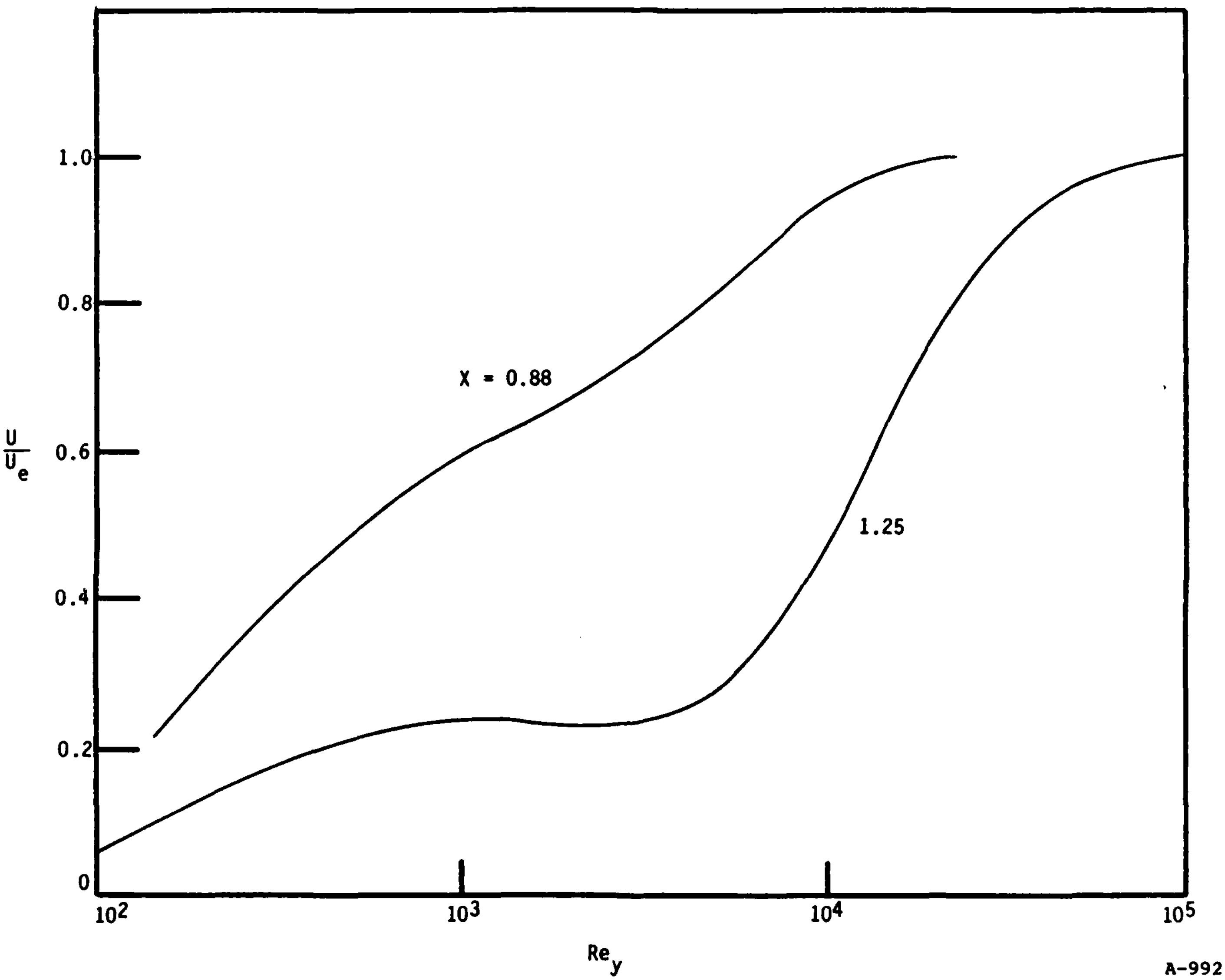

Figure 19. Computed mean velocity profiles at two stations

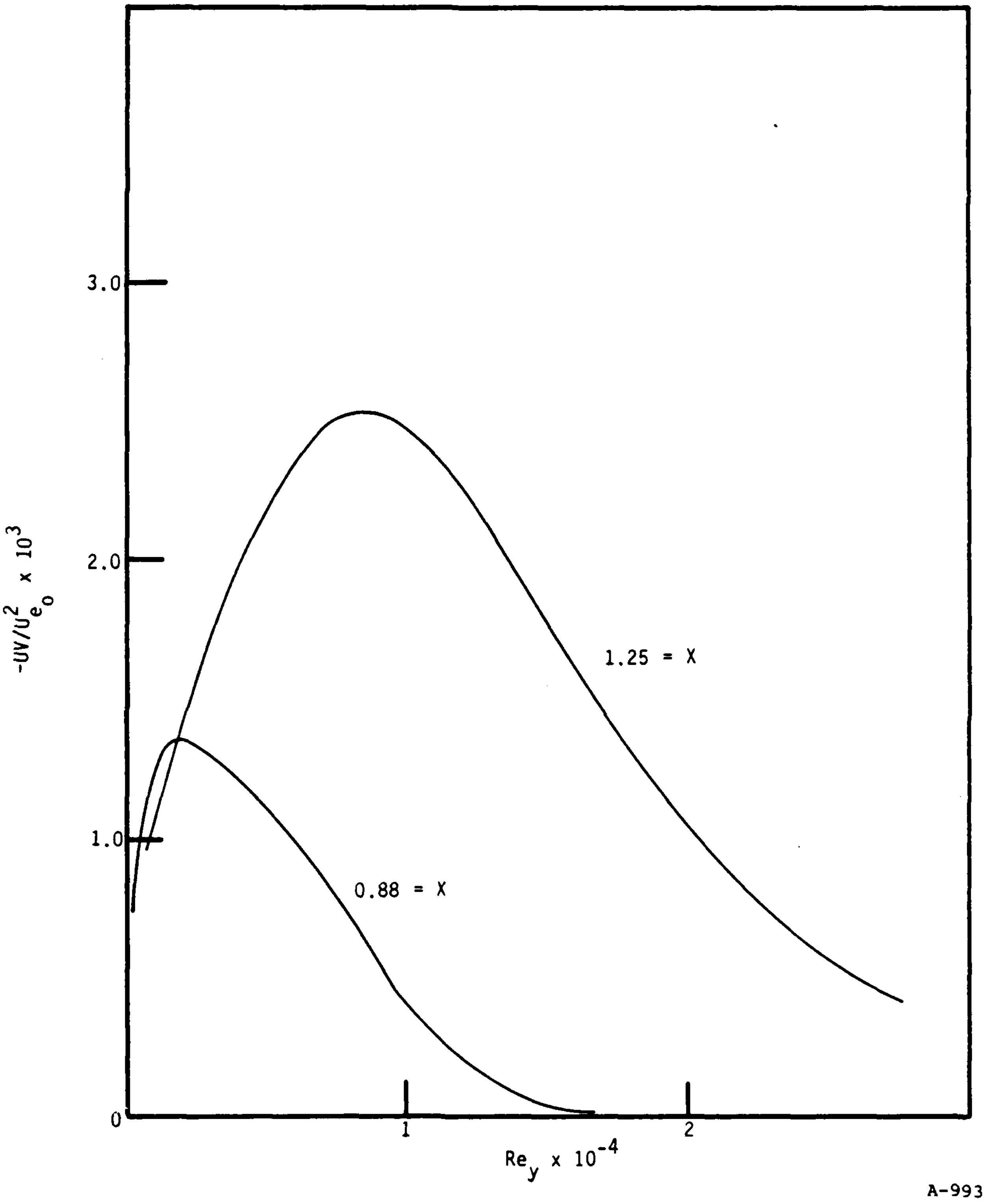

Figure 20. Computed Reynolds stress profiles at two stations

experiments of Bradshaw[19] and Samuel and Joubert,[20] discussed above. An obvious issue is the sensitivity of these results to the turbulence modeling closure assumptions and approximations.

The most surprising aspect of our turbulence solutions in adverse pressure gradients is the amplification of the Reynolds stress that was discussed above in connection with the Bradshaw and Samuel and Joubert experiments, and with the present attempt to reproduce Carter's separated flow solution. This suggests a shortcoming in the turbulence closure modeling. However, it is not obvious where the difficulty lies. Note that there is no direct pressure gradient ($\partial U/\partial x$) term in the equation for the Reynolds stress equation ($\overline{u'v'}$), in contrast to the equations for the components of the turbulent kinetic energy and the dissipation function. This is a direct result of the tensor form assumed for the so-called pressure-strain terms (same form introduced by Hanjalic and Launder[6]). One could arbitrarily introduce a term in the equation governing $\overline{u'v'}$ to damp turbulence in regions of adverse pressure gradients (i.e., a term that would reduce the magnitude of $\overline{u'v'}$ when $\partial U/\partial x$ is negative). But that would violate the desired tensor character of the pressure-strain term and there is no rational basis for such as approach. The primary role of such terms is dictated by kinematic considerations, and can be derived without recourse to "closure" approximations. We investigated the effect of variations in closure constants appearing in other terms in the five-equation model. Changing the wall term in the dissipation equation, or the turbulent diffusion terms, does not resolve the discrepancies, and would jeopardize agreement with other, more basic data upon which the closure constants are based. Arbitrarily increasing the $\partial U/\partial x$ term in the dissipation equation removes the anomolous velocity profile shown in Figure 19, but this again violates a required tensor variation. However, none of our attempts at varying closure approximations produced results that are qualitatively similar to those obtained by Carter,[16] or even produced a well-defined separation zone.

6. RECOMMENDATIONS FOR FUTURE WORK

It should be clear from the results of this study that the implementation of an inverse boundary layer method for high-speed turbulent separated flows is a more ambitious goal than could be accomplished in this program. We firmly believe that an inverse method can be developed as a useful engineering tool. However, three key areas remain where advances are clearly required.

Turbulence Model - The type of Reynolds stress model employed here should provide a good description of turbulence behavior in the presence of pressure gradients. The use of a five-equation model should account for the influence of pressure gradients on the degree of isotropy, the distribution of energy between the different velocity components, and the Reynolds stress; the simpler two-equation (k-ε) approaches inherently assume an unvarying degree of isotropy and should be less accurate. However, comparisons of results of the present five-equation formulation with measurements on attached boundary layers in adverse pressure gradients are very dissappointing. More experiments, particularly on supersonic boundary layers, are clearly in order. Also, some rethinking of the basic formulation of current Reynolds stress modeling is needed. For example, it may be necessary to account for anisotropic dissipation effects and/or varying turbulence length scales in different directions in the presence of strong pressure gradients.

Inverse Boundary Layer Methods - A truly acceptable method for performing inverse boundary layer computations has yet to be developed. The current methods (at least for specified displacement thickess) require several times as much computational effort as the corresponding direct calculation. More iterations are required, and there are various step size constraints. In our experience, the inverse computation is not very "robust".

The primary complication with the inverse approach lies with the displacement thickness. This quantity controls the interaction between the inner viscous region and the outer inviscid region, so the displacement

thickness is the input of interest for the inverse solution, rather than skin friction or mass flux within the boundary layer. Unfortunately, δ^* is defined by an integral across the boundary layer. It does not naturally appear as a boundary condition or as a coefficient in the boundary layer equations. Carter's approach introduces δ^* into the pde's, but in the form of a small difference of large numbers. Cebeci's[13] formulation involves a complex iterative Newton's method (matrix inversion), and our method requires an additional (brute force) iteration. The approach of Cebeci, Keller and Williams[14] is difficult to extend to compressible flows. Clearly, an improved approach is necessary if the inverse method is to find wide application.

Iteration Between Viscous/Inviscid Flows - A final requirement is a reliable algorithm for matching the boundary layer solution to the outer inviscid flow. Existing coupled solutions to date have been for transonic flows, and have been obtained by trial and error iterations. Wigton and Holt[12] have established the theoretical foundation for a method to couple the inner and outer flows, but no algorithms have been developed for hypersonic flows. We had so much difficulty with the inverse method that it was not possible to even address this issue in this effort. Since the Newtonian approximation (pressure proportional to the square of the sine of the local body angle) should be accurate for most hypersonic conditions, it is tempting to expect that an algorithm based on the local derivative of δ^* can be developed. On the other hand, upstream influence transmitted through the separation zone may necessitate a more complex algorithm. If a relatively straightforward algorithm is not possible, then boundary layer methods will not prove to be useful for thin separated flows.

Our experience with the coupling schemes found in the literature (Carter[16], Wigton and Holt[12]) was not very satisfying for our hypersonic boundary-layer interactions. The initial attempts at utilizing the rational Wigton and Holt scheme have proved to be inadequate. Wigton[22] himself abandoned his scheme in favor of Carter's[16] simpler method when solving three-dimensional transonic-wing viscous-inviscid interaction problems. These calculations necessitated hundreds of iterations to convergence; some even

took 10^3 cycles to obtain acceptable answers. The methods indicated above are local coupling schemes. What is needed to tame the iteration cycles is a global scheme wherein changes in the displacement thickness (or boundary-layer mass transpiration $\rho u \delta^*$) influence changes along the entire boundary layer. Local coupling schemes may encounter difficulties due to their inability to enforce a downstream boundary condition (Wigton[23]). Werle and Vatsa[24] have anticipated these difficulties and specified a downstream boundary condition in order to compute interacting supersonic laminar boundary-layer separations with a time-dependent ADI technique. New coupling algorithms must face the global nature of these interaction problems before inverse methods will prove to be useful for separated turbulent flows.

REFERENCES

1. Shang, J. S., Hankey, W. L., Jr., and Law, C. H., "Numerical Simulation of Shock Wave - Turbulent Boundary-Layer Interaction," AIAA J., 14, 1451 (1976).

2. Viegas, J. R. and Horstman, C. C., "Comparision of Multiequation Turbulence Models for Several Shock Boundary-Layer Interaction Flows," AIAA J., 17, 811 (1979).

3. Finson, M. L., "On the Application of Second-Order Closure Models to Boundary Layer Transition," AGARD Conference on Laminar-Turbulent Transition, AGARD Conference Proceedings No. 224, pp. 23-1 to 23-6 (October 1977).

4. Finson, M. L., "A Model for Rough Wall Turbulent Heating and Skin Friction," AIAA Paper 82-0199, AIAA 20th Aerospace Sciences Conference, Orlando, FL (1982).

5. Rotta, J., "Statistische Theorie nichthomogener Turbulenz," Zeitschrift fur Physik., 129, 547-572 (1951), and 131, 51-77 (1951).

6. Hanjalic, K. and Launder, B. E., "A Reynolds Stress Model of Turbulence and its Application to Thin Shear Flows," J. Fluid Mech., 52, 609-638 (1972).

7. Launder, B. E., Reece, G. J., and Rodi, W., "Progress in the Development of a Reynolds-Stress Turbulence Closure," J. Fluid Mech., 68, 537-566 (1975).

8. Finson, M. L. et al., "Advanced Reentry Aeromechanics Interim Scientific Report," Report PSI TR-10, AFOSR-TR-74-1785, Physical Sciences Inc. (1974).

9. Horstman, C. C. and Owen, F. K., "Turbulent Properties of a Compressible Boundary Layer," AIAA J., 10, 1418-1424 (1972). Also Mikulla, V. and Horstman, C. C., AIAA Paper No. 75-119 (1975).

10. Reyhner, T. A. and Flugge-Lotz, I., "The Interaction of a Shock Wave with a Laminar Boundary Layer," Technical Report No. 163, Division of Engineering Mechanics, Stanford University, Stanford, CT (1966).

11. Catherall, D. and Mangler, K. W., "The Integration of the Two-Dimensional Laminar Boundary-Layer Equations past the Point of Vanishing Skin Friction," J. Fluid Mechanics, 26 (1966).

12. Wigton, L. B. and Holt, M., "Viscous-Inviscid Interaction in Transonic Flow," AIAA Paper 81-1003, presented at the AIAA 5th Computational Fluid Dynamics Conference (1981).

13. Cebeci, T., "An Inverse Boundary-Layer Method for Compressible Laminar and Turbulent Boundary Layers," J. Aircraft, 13, 709 (1976).

14. Cebeci, T., Keller, H. B. and Williams, P. G., "Separating Boundary-Layer Flow Calculations," J. Comp. Physics, 31, 363 (1979).

15. Cebeci, T. and Stewartson, K., "On the Calculation of Separation Bubbles," J. Fluid Mech., 133, 287 (1983).

16. Carter, J. E., "Inverse Boundary-Layer Theory and Comparison with Experiment," NASA Technical Paper 1208 (September 1978).

17. Briley, W. R., "A Numerical Study of Laminar Separation Bubbles Using the Navier-Stokes Equations, J. Fluid Mech., 47, pt. 4, 713-736 (June 1971).

18. Tucker, H. J. and Reynolds, A. J., "The Distortion of Turbulence by Irrotational Plane Strain," J. Fluid Mech., 32, 657 (1968).

19. Bradshaw, P.: The Response of a Constant-Pressure Turbulent Boundary Layer to the Sudden Application of an Adverse Pressure Gradient. NPL Aero Rep. 1219, Brit. A.R.C. (1967).

20. Samuel, A. E. and Joubert, P. N., "A Boundary Layer Developing in an Increasingly Adverse Pressure Gradient," J. Fluid Mech., 66, 481 (1974).

21. Lewis, J. E., Gran, R. L., and Kubota, T., "An Experiment on the Adiabatic Compressible Turbulent Boundary Layer in Adverse and Favorable Pressure Gradients," J. Fluid Mech., 51, 657 (1972).

22. Samant, S. S. and Wigton, L. B., "Coupled Euler/Integral Boundary-Layer Analysis in Transonic Flow," AIAA Paper No. 83-180b, presented at the AIAA Applied Aerodynamics Conference, July 13-15, 1983, Danvers, MA.

23. Wigton, L., Private Communication, July 1983.

24. Werle, M. J. and Vatsa, V. N., "New Method for Supersonic Boundary-Layer Separations," AIAA J. 12, No. 11, November 1974, 1491.